Princeton Plasma Physics Laboratory

PPPL-4250

PPPL-4250

Contemporary Instrumentation and Application of Charge Exchange Neutral Particle Diagnostics in Magnetic Fusion Experiments

S.S. Medley, A.J.H. Donné, R. Kaita, A.I. Kislyakov,
M.P. Petrov, and A.L. Roquemore

July 2007

Prepared for the U.S. Department of Energy under Contract DE-AC02-76CH03073.

Princeton Plasma Physics Laboratory
Report Disclaimers

Full Legal Disclaimer

Trademark Disclaimer

PPPL Report Availability

Princeton Plasma Physics Laboratory:

http://www.pppl.gov/techreports.cfm

Office of Scientific and Technical Information (OSTI):

http://www.osti.gov/bridge

Related Links:

U.S. Department of Energy

Office of Scientific and Technical Information

Fusion Links

Contemporary Instrumentation and Application of Charge Exchange Neutral Particle Diagnostics in Magnetic Fusion Experiments

S. S. Medley[a)], A. J. H. Donné[b)], R. Kaita[a)], A. I. Kislyakov[c)], M. P. Petrov[c)] and A. L. Roquemore[a)]

[a)] *Princeton Plasma Physics Laboratory, Princeton, NJ 08543, USA*

[b)] *FOM-Institute for Plasma Physics Rijnhuizen, Association EURATOM-FOM, Trilateral Euregio Cluster, PO Box 1207, 3430 BE Nieuwegein, The Netherlands*

[c)] *A.F. Ioffe Physical Technical Institute, St. Petersburg 194021, Russia*

Email: *medley@pppl.gov*

Abstract

An overview of the developments *post-circa* 1980's of the instrumentation and application of charge exchange neutral particle diagnostics on Magnetic Fusion Energy experiments is presented.

1. Introduction

The methodology of charge exchange neutral particle diagnostic techniques in Magnetic Fusion Energy (MFE) experiments was developed in the early sixties [1, 2] on Russian tokamaks and applied initially for measurements of ion temperature. In that era the role of this diagnostic was to study the ion energy balance in Ohmically-heated tokamak plasmas [3]. Since that time the situation in tokamaks has changed dramatically. With the increase of plasma density and dimensions and usage of auxiliary ion heating by Neutral Beam (NB) injection and Ion Cyclotron Resonance Heating (ICRH), tokamak plasmas became optically thick for thermal atoms and the ion energy distributions became non-Maxwellian. Neutral particle diagnostics for auxiliary-

heated plasmas up to circa 1980s have been addressed in both comprehensive [4-7] and topic-specific [8,9] publications. Thus it is appropriate for this article to focus on subsequent instrumentation developments in this field.

A number of contemporary publications that contain information relevant to neutral particle diagnostics are of note, such as an extensive review of the behavior of fast ions in tokamak experiments [10] and a diagnostic overview for specific MFE devices [11,12]. The conventional hydrogenic charge exchange processes including gas cells for neutral reionization are well documented in the literature [7,8] as is the analysis procedure for passive and active charge exchange measurements [13] and will not be reviewed here. Also, a review of the design and application of dedicated diagnostic neutral beams [14-19] for active charge exchange measurements is outside the scope of this paper.

2. Charge Exchange Neutral Re-ionization Techniques

Two methods for re-ionization of the incoming neutral particles are commonly used in neutral particle analyzers. Gas stripping cells [6] require line-integral densities sufficiently large for adequate ionization but not so large that excessive scattering occurs. Conductance restricting input and exit apertures are required to limit gas loading and differential vacuum pumping between the stripping cell and the remainder of the apparatus is generally necessary. The stripping cell apertures limit the acceptance solid angle and thus the available signal strength. An alternative method is to use ultra-thin foils [20] (typically 50 – 100 Å carbon) that are mechanically supported on a high-transparency metallic mesh. In recent years, it became possible to use so called diamond-like carbon stripping foils that are much stronger than usual carbon foils [21]. Stripping foils relax vacuum pumping requirements and constraints on the acceptance solid angle but have relatively low stripping efficiency and large scattering below energies of ~ 10 keV. Unlike gas stripping cells, stripping foils are subject to energy

loss that can vary from one particular application to another but is of order $\Delta E \approx 4.4 \times 10^{-3} d\sqrt{E}(keV)$ for hydrogenic ions in the energy range of tens of keV. Foils are thus generally less efficient than gas cells for providing usable re-ionized neutral flux at hydrogenic energies below ~ 10 keV. However, the stripping efficiency of the foils for energies E < 10 keV can be significantly increased with the use of acceleration of secondary ions after stripping (see Section 5).

3. Electrostatic Spectrometers

In contemporary tokamaks and other magnetic confinement devices involving either single species plasmas or disparate thermal and non-thermal ion energy distributions associated with the use, for example, of neutral-beam injection and radio-frequency auxiliary heating, Neutral Particle Analyzer (NPA) techniques possessing energy resolution but not mass resolution are appropriate. Electrostatic energy analyzers with a variety of geometries including cylindrical plate [20,22-26], parallel plate [27,28], or retarding-potential systems that are appropriate for low energy measurements [29] are suitable for such applications. Small-angle (30° – 90°) cylindrical plate devices have relatively low energy resolution ($\Delta E/E$ ~ 10% - 40%) and no focusing in the plane of deflection but have economy of size and simplicity of construction. The 127° design has superior focusing and energy resolution (< 10%) but have more critical construction tolerances. The parallel plate system has the advantage that multiple detectors can be positioned along various trajectories between plates having constant applied voltage to get multiple energy channels.

As an example of the cylindrical plate method, a unique spatially imaging NPA diagnostic, built for the Fast Ion Diagnostic Experiment (FIDE) [22] on the Poloidal Divertor Experiment (PDX), is presented in Fig. 1a. This device has a pinhole camera type of input geometry in the horizontal plane, followed by a fan-geometry stripping cell illustrated in Fig. 1b that preserves the spatial information of the "camera". Ions emerging from the stripping cell are deflected in the vertical direction by a 127° cylindrical plate electrostatic energy analyzer and focused on a large area micro-

[1]channel plate (MCP) array. The MCP array has a multi-anode particle collector whose output feeds an array of amplifiers giving spatially and temporally resolved measurements of the charge exchange efflux. The total system has ~ 1 cm spatial resolution, 3% energy resolution and down to 10 microsecond time resolution.

The theoretical relationship between the energy E of the detected particles of charge Z and the deflection plate voltage V is $E = V \bullet Z/\ln(b/a)$ assuming infinitely tall cylindrical deflection plates and near-circular particle orbits. Here, *a* and *b* are the radii of the inner and outer plates, respectively, which are at the potentials ± V. Taking δR to be a variation of the central particle trajectory R = (*a* + *b*)/2, a simple estimate for the energy resolution δE/E is given by $\delta E/E \approx \delta R/R$. The variation δR and hence δE can be controlled by inserting a slit of suitable width at the exit of the cylindrical plates provided energy straggling is minimal.

Passive charge exchange measurements were obtained on PDX to investigate "fishbones" [30] as shown in Fig. 2 [31]. The upper panel shows FIDE charge-exchange spectra from PDX device for a no-fishbone discharge (2 beams) compared with a severe-fishbone discharge (4 beams). The depletion of beam ions in the region $E_{inj/2} < E < E_{inj}$ is evident where $E_{inj} \sim 46$ keV.

In Fig. 2, the spikes in the spectra over the noted energy region result from the expulsion of beam ions during fishbone bursts to the plasma edge. The large signal results from charge exchange in the high neutral density in the edge region. Note that these spectra were obtained by periodically sweeping the plate voltage of the NPA, so that the distance between the spikes reflects their separation in time rather than localization in energy. The lower panel shows simulations of the spectra using a bounce-averaged Fokker-Planck code with a fishbone model that reproduce the beam ion losses observed experimentally.

The FIDE diagnostic on PDX also featured a collimated, scanning diagnostic neutral beam to deposit ions on orbits as illustrated in Fig. 3. The orbits correspond to

[1] *Note that in this paper, the source of the figures is acknowledged by the reference appended to the caption.*

ions from the full, half, and third energy components of the beam, which was modulated to permit “phase-locked” detection with the spatially imaging NPA. By determining the orbit shifts, this approach was employed to obtain the time-evolving q-profile measurements [23] shown in Fig. 4.

4. Superimposed E||B Spectrometers

The advent of fusion experiments involving multi-species plasmas containing both thermal and non-thermal ion energy distributions driven by neutral beam and radio-frequency heating has driven significant changes in the requirements for many MFE plasma diagnostics. In the area of charge exchange diagnostics, this imposed a need to extend the capabilities of spectrometers used for neutral particle analysis. With beam heating, the need for mass resolution became prevalent, due to the fact that two-ion component plasmas became commonplace wherein the energy distributions of the beam slowing-down particles and the Maxwellian plasma bulk ions strongly overlapped. Frequently the hydrogenic ion species for the beam and target plasma were different. In cases where they were the same (e.g. D-D), the residual population of other ions (e.g. H) could often be exploited for ion temperature measurements.

In early devices, to provide both mass and energy analysis capability for charge exchange spectrometers the initial approach was to utilize a magnetic field region for momentum analysis followed by an electrostatic system (typically cylindrical [33] or parallel plate [34] condensers) for energy analysis. In such configurations, the magnetic and electric fields were orthogonal to each other and the resulting instrument had several disadvantages: a) the cylindrical condensers were complicated to fabricate and align, b) the spatially separated magnetic and electrostatic field regions led to relatively large spectrometer dimensions, and c) typically only a single ion species was detected

at a time because there were too few channels (~ 5-7) to provide useful measurements of more than one ion species.

The requirements for the charge exchange system for the Tokamak Fusion Test Reactor (TFTR) and the Joint European Torus (JET) experiments were considerably more involved than for preceding devices due to the provision for operation using combinations hydrogen, deuterium, or tritium for either the neutral beam injectors or the target plasma. Also, production of energetic ions tails using ICRF heating of H, ^{3}He, and T minorities needed to be accommodated. For TFTR, a novel charge exchange neutral analyzer concept, using a dee-shaped region of parallel electric and magnetic fields (E||B), was developed at the Princeton Plasma Physics Laboratory (PPPL) [35]. This spectrometer was designed to measure the mass-resolved energy distributions of both the thermal ions and the supra thermal populations arising from neutral beam injection and ion cyclotron radio frequency heating.

The basic operating principle of the E||B spectrometer is illustrated in the top panel of Fig. 5. After re-ionization of the charge exchange neutrals in the stripping cell, the ions enter perpendicularly into a semi-circular region of parallel magnetic and electric fields. In these fields, the Lorentz forces

$$m d\underline{v}/dt = q \times (\underline{v} \times \underline{\mathrm{B}} + \underline{E}) \qquad (1)$$

are not coupled. While traversing an arc of 180$^{\mathrm{o}}$ due to the magnetic field $\underline{\mathrm{B}}$, the ions are displaced parallel to the electric field $\underline{\mathrm{E}}$. The time-of-flight

$$t_j = (\pi/\mathrm{B})\left[m/e\right]_j \qquad (2)$$

between entering and exiting the field region is independent of the initial velocity for any given ion species $(m/e)_j$. The displacement Y_j of the j-th species parallel to the electric field is given by

$$Y_j = (\pi^2/2)\left[E/B^2\right]\left[m/e\right]_j \qquad (3)$$

that is also independent of velocity, so that all particles of a given m/e ratio are displaced along the electric field direction by the same amount. The ion species $(m/e)_j$ entering with velocity v_k are displaced along the detector plane a distance

$$Z_{jk} = (2/B)\left[m/e\right]_j v_k \qquad (4)$$

from the entrance point in a direction perpendicular to $\underline{v}_k$ x $\underline{B}$. The collection plane thus exhibits parallel columns of analyzed ions, each column containing the energy dispersed ion of a given (m/e) ratio. The detector is located in the collection plane and consists of a planar microchannel plate (MCP) [36] that is provided with three rectangular, semi-continuous active area strips, one coinciding with each of the mass rows for detection of H^+, D^+, and T^+. Each strip is divided into multiple elements of width ΔZ_j. The energy resolution

$$\Delta E/E = \pm \Delta Z_j / Z_j \qquad (5)$$

where $E = mv_k^2/2$ is therefore a function of displacement along each mass column.

In Fig. 5, the bottom panel shows plan and elevation cross-sections of the EIIB analyzer with the inset (not to scale) showing the geometry of the MCP detector. The smaller chamber houses a 25 cm long stripping cell typically operated at 1-3 mTorr helium while the main chamber contains the field region and the detector. The electric

field is produced between one magnet pole face at ground potential and a negatively biased, dee-shaped electrode mounted against, but electrically insulated from, the opposite pole face. The ion beam enters near the ground electrode for two reasons. First, this location reduces perturbation of the incoming particle energy due to the electrode potential. Second, this arrangement permits utilization of the full separation of the magnet gap. The MCP detector array is provided with three rectangular, semi-continuous active area strips, one coinciding with each of the mass rows for detection of H^+, D^+, and T^+ and each mass row has 39 energy channels.

The analyzer was calibrated from 0.5 to 150 keV for both hydrogen and deuterium to determine the energy, energy resolution, and total detection efficiency for a range of analyzer magnetic and electric field setting. Prior to the start of TFTR operation, an EIIB prototype [37] was operated on the Princeton Large Torus (PLT) to validate the design, including the ability to measure "mass 3" particles during Helium-3 minority radio frequency heating experiments [38]. The EIIB spectrometer has an energy range of $0.5 \leq A(amu)E(keV) \leq 600$. The FWHM energy resolution varied from $\Delta E/E = 7\%$ at the low energy region of the MCP to $\Delta E/E = 3\%$ at the high end. The energy dynamic range was $E_{max}/E_{min} = 30$, where E_{max} and E_{min} are the maximum and minimum energies that can be measured simultaneously and the mass rejection between adjacent mass columns was ~ 1000:1. A broad range of ion-related phenomena was investigated such as the ion temperature in Ohmic and neutral beam heated discharges [35], adiabatic toroidal compression experiments [39], fast ion radial diffusion [40], and MHD effects such as fishbones [41].

During high power deuterium neutral beam heating of deuterium plasmas in TFTR, charge exchange measurement of the central ion temperature was difficult because the deuterium neutral energy spectrum overlapped the deuterium neutral beam slowing-down spectrum, and there was insufficient residual hydrogen [$H/(H + D) \leq 1.5\%$] to obtain a measurement from the background plasma. A solution was developed that

involves fitting the deuterium slowing-down spectrum obtained at energies above the neutral beam injection energy [42], as illustrated in Fig. 6. Competition between ion energy diffusion and electron drag can give rise to a slope of the ion energy distribution above the neutral beam injection energy of the form f(E) ~ exp(-E/T_{eff}), where T_{eff} given by

$$T_{eff} = \frac{T_i + (E/E_{crit})^{3/2} T_e}{1 + (E/E_{crit})^{3/2} \pm \tau_{se} 9.58x10^{11} \frac{Z_b}{A_b} \frac{|\vec{E^*}|}{v_b} (E/E_{crit})^{3/2}} \quad (6)$$

is an effective temperature that is a weighted average of the ion and electron temperatures. E_{crit}, the critical energy at which ions and electrons receive an equal energy transfer from the beam ions, is given by

$$E_{crit} = 14.8 A_b T_e \left(\frac{[Z_i]}{A_i}\right)^{2/3} \quad (7)$$

where the average charge to mass ratio of the bulk ions (denoted by the subscript *i*) is

$$\frac{[Z_i]}{A_i} = \frac{\sum_j n_j (Z_j^2/A_j) \ln \Lambda_j}{n_e \ln \Lambda_e} \quad (8)$$

and the subscript *j* indexes the bulk and impurity ion species. The last term in the denominator of Eq. (6) which accounts for the effect of the toroidal electric field, $|\vec{E^*}|$, is usually small (O ~ 10^{-2} compared with unity) and can be neglected. Here the "±" sign corresponds to neutral beam injection parallel (-) or anti-parallel (+) to the toroidal electric field.

The ion temperature determined in this manner represents the central ion temperature if the neutral beam deposition and the measured charge exchange neutral flux are core-weighted. In TFTR, these requirements were satisfied. An example of the ion temperature measurements obtained with this technique is shown in Fig. 7.

The superimposed EIIB spectrometers constructed and calibrated at PPPL have been applied to charge exchange neutral particle measurements on ATF [43], LHD [44], NSTX [45] and MAST [46]. A similar instrument was developed for TMX-U [47]. On NSTX, the horizontally and vertically scanning NPA diagnostic views across the co-injection paths of the three neutral beam lines and was applied to thermal ion temperature [48] and energetic ion measurements including the effects of High Harmonic Fast Wave (HHFW) heating [49] and MHD activity [50] on the energetic ion distribution. Active charge exchange measurement of the ion temperature shown in Fig. 8 compares well with data from the charge exchange recombination spectroscopy diagnostic. The horizontal scanning enables measurement of the NB anisotropic energy distribution, as illustrated in Fig. 9. This spectrum was derived from energy distributions measured on a shot-to-shot basis. The spectrum is highly anisotropic with the ion population depleting with decreasing NPA tangency radius. This occurs because decreasing tangency radius corresponds to viewing trapped ions whose population is small because the co-injected tangential NB deposits ions primarily on passing orbits. Evidence of spectrum 'fill' below the critical energy, $E_{crit} \sim 15$ keV due to pitch angle scattering can be seen.

The superimposed EIIB spectrometer, however, does have some disadvantages. Adequate spatial separation of the H^+, D^+, and T^+ ion species results in a relatively large magnet gap. From the relation for the magnetic field strength B(Gauss) = 1.25 (NI/d), it is evident that to provide a specified field using a set number of coil turns, N, the required energizing current I(A) is proportional to the pole separation d(cm). In addition to the sizable magnet power requirements arising from a large pole gap, the associated fringe field might be expected to adversely affect the ion trajectories. Alternative configurations are possible which reduce the pole separation while preserving the EIIB analyzer concept. Some degree of reduction in pole separation

can be achieved by requiring that only part of the necessary spatial dispersion of the ion species occurs while the ions are traversing the poles. The remainder of the dispersion is realized by allowing the ions to drift some distance on exiting the field region before striking the detector. If the detector plane remains parallel to, but is displaced away from the straight edge of the magnet, the mass columns become parabolic in shape with lower energies having a greater displacement in the direction of the electric field. Linear mass columns may be recovered, however, by tilting the detector plane about an axis that is parallel to the field direction and passes through the "entry point" of the ions into the magnet gap [51]. The greatest reduction in pole separation is achieved by applying the electric field after the ions emerge from the magnetic field.

5. Tandem EIIB Spectrometers

A variation of the superimposed EIIB concept in which the parallel magnetic and electric fields were spatially separated was developed for the charge exchange analyzers on the Poloidal Divertor Experiment (PDX) [13], replacing an earlier design based on cylindrical electrostatic plates [33]. Since then, additional variations have improved on the PDX the design [34, 35]. A schematic illustrating the concept is shown in Fig. 10. The re-ionized neutral particle influx first enters the magnetic field region (A) and undergoes momentum analysis. Typically the magnet pole pieces are mounted on the top and bottom lids on the vacuum chamber with the electrical windings sealed outside the vacuum. The vacuum chamber walls are constructed of soft iron that provides both a return path for the magnet flux and a magnetic shield against the ambient fields of the MFE experimental device. Ions emerging from the magnet then enter a parallel plate condenser (B) that is oriented so that the electric field is parallel to the magnetic field: i.e. tandem EIIB. The condenser consists of a pair of parallel plates with one biased negatively and the other being a ground plane that is mounted slightly

below the bottom magnet face. The geometry of the electrostatic plate is chosen to allow the flight time of an energetic ion to be equal for all particles of the same mass that exit from the magnet. The vertical displacement is then proportional to the acceleration in the electric field and dependent only on the mass of a particle and not its energy (assuming q = 1). This allows a semi-linear array of detectors (C) to view particles of the same mass while mounted at approximately the same height above the centerline of the magnet poles. With this geometry, the magnetic field in effect selects the desired energies and the electrostatic deflection separates these energies into one or more rows of different mass. By choosing the proper deflection voltage for a given magnetic field, the desired mass species may be selected. Due to the relatively large spatial extent of the detector plane, discrete channel electron multiplier detectors are usually employed rather than spatially continuous MCP detectors. This restricts the number of energy channels that can be provided compared with superimposed EIIB-type spectrometers [35]. By switching between positive and negative biasing of the electrostatic condenser, a usually dormant space in a tandem EIIB instrument can be exploited to install additional detector arrays and extend the accessible mass and energy range [52].

The PDX-style tandem EIIB spectrometers built at PPPL were implemented on Alcator C-Mod [53] and Tokamak de Varennes [54]. Similar instruments utilizing and making improvements on the PDX concept have been developed for JT-60 [55], JET [56], and JFT-2 [57]. Tandem EIIB analyzers decommissioned from JET were deployed on ASDEX [58], Tore Supra [59] and other experiments. At the A. F. Ioffe Physical-Technical Institute, a tandem EIIB neutral particle analyzer specialized for high-energy measurements was developed [60] and deployed on TFTR [61], JET [62] and JT-60U [63].

The evaluation of the hydrogenic isotope ratio using neutral particle emission is a delicate task during auxiliary heating both with NBI and ICRH since neutral spectra can

be dominated either by slowing-down ions or by fast ion tails. Measurement of the isotope ratio is particularly important in the case of DT experiments in order to evaluate fusion reactivity.

An advanced tandem EIIB instrument called ISEP (Ion Separator) to measure hydrogenic isotope ratios was developed at the A. F. Ioffe Physical Technical Institute and deployed on JET [64]. The ISEP NPA has excellent H/D/T mass separation (with rejection of neighboring masses $< 10^{-3}$) and high detection efficiency (up to 100% for higher energies) in the energy range 5 - 740 keV for H^o, 5 - 370 keV for D^o and 5 -250 keV for T^o.

As shown in Fig. 11, the ISEP NPA consists of three main parts: accelerator chamber, magnet chamber and detector chamber. ISEP has the following specific features: a) stripping of neutral atoms using a thin diamond like carbon foil, b) acceleration of the secondary ions after (up to 100 kV) to compensate scattering after stripping and to get sufficient signal-to-background ratio in DT experiments, c) EIIB analysis of ions in specially designed non-uniform electric and magnetic fields providing two dimensional focusing in the dispersion system and therefore high detection efficiency for ions, d) ISEP detectors have high sensitivity for hydrogenic ions (~ 1) and simultaneously very low sensitivity for neutron and gamma radiation ($< 10^{-7}$).

The ISEP detectors consist of CsI(Tl) scintillator material sputtered onto thin quartz glass (0.5 mm) that is optically coupled to the entrance window of Hamamatsu R2248 photomultipliers. The scintillator thickness is ~ 1- 7 μm depending on the energy of ions detected in a particular energy channel. The stopping distance of ions in the scintillator material is approximately equal to the thickness of the scintillator. This provides simultaneously the maximal ion detection efficiency and the minimal neutron/gamma sensitivity. The neutron and gamma sensitivity of the ISEP detectors has been measured experimentally with the use of a radioactive source.

To simulate the background radiation of a high temperature plasma, a ^{252}Cf radioactive source has been used that generates neutrons having a continuous energy

spectrum with $E_{max} \sim 10$ MeV and an average energy $\langle E \rangle_n = 2.2$ MeV. The neutron emission is accompanied with ~ 1 MeV gamma radiation (2.7 gammas per neutron). This source simulates well the neutron and gamma emission generated in fusion plasmas. The results of those tests are shown in Fig. 12 where the detector integral pulse height spectra generated by the ^{252}Cf neutron source are presented in terms of the neutron-gamma sensitivity (one neutron or gamma per detector pulse) versus ADC threshold. The threshold values are plotted in terms of the energy scale of H^+ ions. (Note that for the energies E ~ 5 keV and higher the sensitivity of the detector to H^+ is equal to ~ 1.0)

The five curves plotted in Fig. 12 correspond to a photomultiplier tube (PMT) without scintillator and to PMTs with four values of scintillator thickness ranging from 1.1 μm scintillator (as used in the lowest energy ISEP channels) to 7.0 μm (as used in the highest energy channel). The curves show that the neutron and gamma sensitivity is higher for thicker scintillator material and decreases by 2-3 orders for magnitude in the energy range 10 – 100 keV. This effect justifies the application of ion acceleration before detection. Calculations made on the basis of Fig. 12 show that 80 – 100 kV acceleration leads to an increase of signal-to-background ratio by three orders of magnitude for low energy H^+ ions and by more than two orders of magnitude for high-energy H^+ ions due to the good separation of ion pulse amplitudes from the background signal.

The ability of ISEP detectors to count ions in the presence of intensive neutron and gamma radiation on JET is illustrated in Fig. 13 [64]. Shown is a computer code simulation of the ISEP detector pulse height distribution for the detection of D^+ ions in the presence of DT neutron radiation. The parameters used in the simulation were: ion energy $E_d = 5$ keV, acceleration voltage $U_{ac} = 80$ keV (total energy $E_D = 85$ keV) and a D^+ count rate of 10^4 s^{-1}. The total neutron emission rate normalized to JET DT experimental conditions varies from $1x10^{17}$ to $5x10^{18}$ n/s (neutron flux = $1x10^9$ – $5x10^{10}$ $n/cm^2/s$ at the ISEP location). In the simulation, the experimentally measured neutron sensitivity (Fig. 12) and energy resolution ΔE of the detector ($\Delta E / E = 35 – 52$ % for

different PMTs) was used. The pile up effect of small neutron pulses was taken into account in the simulation. This effect plays a very important role in the formation of pulse height distributions for high values of neutron emission. It is seen that even in the presence of a background emission rate $2x10^{18}$ n/s, the D^+ signal (E = 5 keV) can still be distinguished. Note that no neutron shielding of the detectors has been taken into account in these calculations.

In order to obtain good focusing of secondary ions in ISEP, it was necessary to use specially designed non-uniform magnetic and electric fields. The non-uniform magnetic field was obtained using a non-uniform gap between the magnet poles (see Fig. 11). A condenser of a special two-dimensional shape as shown in Fig. 11 produces the non-uniform electric field. Fig. 14 shows the intensity of the ISEP magnetic field versus the distance from the entrance edge of the magnet. Open circles are measurements made by a Hall probe whereas the solid line is calculated. It can be seen that the calculation and measurements are in good agreement.

An example of a hydrogenic isotope ratio measurement on JET is shown in Fig. 15 in which experimental (data points) and calculated spectra (curves) deuterium and hydrogen atom spectra are shown for a JET NB heated high-density plasma. In this discharge, central electron density $n_e(0) = 9.6x10^{13}$ cm^{-3} and central electron temperature $T_e(0) = 5.06$ keV. The central ion temperature derived from a comparison of the calculated and the experimental atom spectra was $T_i(0) = 15$ keV. In the modeling [64] it was assumed that the deuterium and hydrogen temperatures were equal. The measurements presented in Fig.15 and corresponding modeling give a value of the isotope composition over the JET plasma radius of n_H/n_D = const (r/a)=0.1. It would be incorrect to derive the n_H/n_D value directly from the curves presented in Fig.15 because the plasma transparency for H and D atoms is different. The modeling takes this into account. The deviation of the deuterium points with the energies 30.9 keV and 41.3 keV from the calculated spectrum is the result of the influence of slowing down of heating beam particles. This phenomenon can create serious problems for the measurement of hydrogenic isotope ratios in the case of NB heated plasmas.

The ISEP NPA has been applied to study the ion transport in the JET plasma during the Tritium Trace Experimental (TTE) campaign [65]. Special features of the experiment such as the low tritium background in the plasma, the small tritium influxes from the wall and the purity of deuterium neutral beam injection all contributed to the very high contrast of the neutral tritium fluxes due to small T_2 puffing. The ISEP NPA was installed 28 cm above the tokamak mid-plane and the observation line viewed the plasma in the horizontal direction.

A typical time evolution of tritium neutral fluxes in JET discharges with reduced T_2 puff is presented in Fig. 16. It was observed that the delay of tritium fluxes from the beginning of the T_2 puff to the peak of the fluxes increased with the particle energy. Estimates of the tritium thermal equilibration time showed that it is relatively short (~ 30 ms). Obviously the slower growth rate of higher energy neutral fluxes is mainly determined by the tritium ion transport. The reason for the delay is that higher energy neutral fluxes come from deeper plasma regions due to the ion temperature increasing towards the center and the higher plasma transparency for more energetic particles. This is illustrated in Fig. 17 by the calculated source functions for different neutral flux energies in this particular JET plasma where it can be seen that 4 keV neutral fluxes are emitted from the peripheral plasma (0.7 - 0.9)*a* and the 28 keV fluxes regions deeper in the plasma (0.2 - 0.6)*a* where '*a*' is the plasma minor radius. After the puff, as ionized tritium atoms penetrate from the plasma edge to the center they give rise to more energetic neutral fluxes. Thus the observed dependence of the delay on the particle energy can be interpreted as propagation of the tritium ions into the plasma to a particular radial position. To estimate the tritium transport coefficients a simple transport model was applied. The tritium flux is expressed as the sum of tritium diffusion and inward pinch terms $\Gamma = -D\frac{\partial n}{\partial r} + Vn$. The coefficients *D* and *V* are assumed to be constant over the plasma radius. Modeling gives a tritium diffusion coefficient of 0.2 m^2/s together with an inward pinch velocity of 1.5 m/s.

Sometimes the spatial constraints on modern plasma facilities dictate the need for a compact NPA. A compact NPA can be installed almost anywhere near a plasma

machine and can be easily moved elsewhere or replaced, if necessary, with another device. A set of several compact analyzers can be used for multi-chord NPA diagnostics. In addition, NPAs used on modern plasma facilities require neutron and γ-ray shielding because detectors (channeltrons, microchannel plates or PMTs) are sensitive to neutrons and γ-rays. A decrease in the NPA size makes it possible to reduce considerably the weight of the magnetic shields as well as neutron and γ-ray shields.

A new compact neutral-particle analyzer (CNPA) has been recently developed at the A.F. Ioffe Physical Technical Institute [66]. The CNPA is a tandem EIIB mass and energy resolving spectrometer for the simultaneous analysis of the hydrogen (0.8 - 80 keV) and deuterium (0.66 - 36 keV) neutral particle fluxes. A thin (100 Å) diamond-like foil is used for stripping instead of the conventional method of stripping in a gas cell. The analyzer magnetic field is produced by two powerful (1 Tesla) NdFeB permanent magnets instead of conventional electromagnets. These two innovations made it possible to considerably decrease the size (169 x 302 x 326 mm) and weight (42.5 kg) of the analyzer. To increase the detection efficiency, the device uses electrostatic acceleration of ions scattered by the stripping foil and provides a magnetic field configuration with two-dimensional focusing. The analyzer has been used in experiments on the Wendelstein 7-AS stellarator, the TCV tokamak, the LHD stellarator, the SSPX dynamo spheromak and the TJ-II stellarator. A diagram of the CNPA is presented in Fig. 18 while Fig. 19 shows the efficiencies for detection of hydrogen and deuterium atomic fluxes. Electrostatic acceleration of ions scattered by the stripping foil provided focusing of the ions before the EIIB dispersion which leads an increase of the detection efficiency in the lower energy range $E < 1$ keV.

6. Time-of-flight Spectrometers

A different approach to devising advanced neutral particle diagnostics is based on the utilization of time-of-flight (TOF) techniques. In principle two main classes of TOF spectrometers can be distinguished: systems for diagnosing neutral particles with

low energy based on measuring the drift time of the particles over a 1.5 – 2.5 long straight flight path, and systems that combine TOF techniques with electrostatic techniques and that are aimed at particles with higher energies.

For a better understanding of processes in the plasma edge (like those occurring at the L-H transition) it is important to diagnose the neutral particles emerging from this region. The energy range of interest for these edge populations (~300 eV and below) cannot be seen by the standard NPAs based on stripping cell or stripping foil techniques. This is because at those energies, the stripping efficiencies are too low to receive high enough a signal. All low energy neutral beam analyzers follow more or less the concept which was introduced at PLT [67] and which is schematically illustrated in Fig. 20. The flow of neutral atoms emerging from the plasma edge is chopped into short bunches by a chopper plate. The energy distribution of the particles within a bunch can be derived from the measured time-of-flight distribution of the particles after having traversed a distance of typically 1.5 – 3.5 m. Detection is usually accomplished by collecting the secondary electrons that are emitted when the neutral atoms impact a Cu or a Cu-Be plate. By accelerating the particles towards a particle multiplier a detection efficiency of almost 100% can be achieved. The secondary emission coefficient of Cu and CuBe varies by two orders of magnitude in the energy range from 10 to 200 eV, and this usually limits the lowest energies at which measurements can be done to several tens of eV

After the first application at PLT [67], similar systems have been used on ASDEX [68, 69], JFT-2M [70], RFX [71, 72], Alcator C-Mod [73], GAMMA-10 [74] and TORTUR [75, 76]. About half of these systems applied a standard chopper plate as depicted in Fig. 20a, the other half used a cylinder with slits mounted on top of a turbo-molecular pump [68]. In all cases the typical opening time of the chopper is ~1-2 μs. The minimum distance between adjacent slits in the chopper is determined by the difference in flight time of the fastest and the slowest neutral particles and amounts to typically 100-250 μs. Hence, only a relatively small fraction of the particles emerging from the plasma is actually analyzed. Most of the choppers applied have an additional optical system with a HeNe laser and a photodiode to yield a trigger signal and to gate the

detector (if needed) during the first few μs after a chopper opening to prevent saturation of the detector by visible and UV light and by x-rays. Because of the low signal levels, one often has to add subsequent spectra to improve the statistics, leading to an effective time resolution in the order of a few ms up to even 20 ms. For JFT-2M [70], neutral gas is puffed into the plasma in front of the TOF analyzer to enhance the signal-to-noise ratio.

The RFX reversed field pinch is equipped with two low-energy TOF NPAs [72], one viewing vertically and one horizontally. In high-density discharges both systems measure the same flux spectrum, but in low-density discharges differences are found (see Fig. 21). The fact that the horizontal NPA measures a higher flux than the vertical one is attributed to the fact that the horizontal system views deeper into the plasma, since the line-of-sight of the vertical system does not pass through the plasma center. The system at Alcator C-Mod [73] is mounted at the back end of a EIIB analyzer, which enables straightforward cross calibration of both systems in the energy range between 0.5 and 4 keV. Additionally the collinear line-of-sight of both systems can be scanned poloidally through the plasma. A special feature of the system applied at TORTUR [75, 76] is the conversion of the neutral hydrogen atoms to H^- ions on a cesiated tungsten plate. The conversion efficiency drops only very gradually and smoothly below 200 eV and still exceeds 5% at 5 eV. Nevertheless attenuation of the hydrogen atom flux from the plasma in the flight tube by elastic scattering on molecular hydrogen gas was found to thwart low-energy atomic hydrogen detection below 10 eV.

An approach developed for diagnosing neutral particles with energies above 1 keV is based on electrostatic TOF analyzer spectrometers. Energy analysis is provided by either parallel [77] or concentric [78, 79] electrostatic plates. Mass selection within the instrument, e.g. H, D, or T, is achieved by time-of-flight measurements using a delayed coincidence technique. In this technique, a thin carbon foil (typically a few $\mu g/cm^2$) is mounted at the entrance of the TOF analyzer. Secondary electrons are emitted when a neutral or a charged particle traverses the foil, and are detected by means of channel electron multipliers (channeltrons or channelplates) to serve as start signal for a time-of-flight measurement. The particle itself generates the stop signal in a

detector at the end of its flight path. This TOF technique was proposed in 1982 [80] and first applied in an energy analyzer used in an active beam experiment at TEXTOR [81, 82].

At the RTP tokamak, the TOF technique was integrated in a parallel plate electrostatic analyzer [77]. In this system the secondary electron emission from the stripping foil was measured in both the forward and backward direction. This together with the stop detector resulted in a triple coincidence technique and, hence, a very low sensitivity for neutron and gamma background radiation. The carbon foil at the entrance of the detector has two functions: stripping the neutral particles and generating the start signal via the secondary electron emission, thus resulting in a rather compact set up. The mass is determined from the measured time-of-flight and, hence, only a single array of detectors is needed in the electrostatic analyzer to resolve energy and mass. The neutral particle flux on the start detector should not become too large (typically $< 6 \times 10^5$ s^{-1}) to avoid too high a dead time of the system.

For the JET tokamak a neutral particle analyzer was developed [78] that combined the TOF technique with an electrostatic analyzer featuring concentric electrodes (see Fig. 22). First the neutral particles are stripped in a gas cell, and then they enter the cylindrical electrostatic plates that deflect the particles over an angle that corresponds to their energy. A system of 15 separate TOF detecting units is used to detect the particles in 15 energy intervals ranging from 0.5 to 250 keV. Each detecting unit consists of a start detector (made up of a carbon foil and a channel electron multiplier (CEM) to detect the secondary electrons from the foil) and a stop detector. The length of the flight tube varies from 11 cm for the low energy channels to 30 cm for the high-energy channels, and is chosen such that particles of different mass are separated by their time of flight. The double coincidence technique also has a high noise rejection capability. The system can register the three different hydrogenic masses simultaneously by means of three delayed time gates in the electronics. In addition to the usual measurement of thermal and energetic ion energy distributions, the hydrogenic isotope ratio can be monitored at JET in the outer half of Ohmic plasmas (see Fig. 23) [83]. The system at JET suffered from a cross talk between the masses,

for which a correction had to be made. The cross talk was attributed to particles scattered in the start foil and reaching the stop detector via one or more collisions with the wall of the flight tube. The cross talk could be largely avoided in a more recent system implemented on the Large Helical Device (LHD), in which a biased diaphragm is used in front of the stop detector [79, 84]. This system features a mass rejection ratio up to 1/1000 and further differs from the system at JET in that it has a larger energy range: 0.5 to 370 keV. The energy resolution is typically 7%. The pitch angle of the TOF analyzer at LHD can be scanned in the toroidal direction from 40° to 100° in a single (100 s long) discharge, with a speed of 0.7° s^{-1} [85]. This makes it possible to observe in detail the pitch angle distribution of energetic ions in neutral beam heated plasmas and to study loss cone effects in the particle population trapped by the magnetic ripple [86].

7. NPA Measurement of MeV Ions

NPA measurements of MeV ions generated, for example, by ICRF minority ion heating or as products of DD and DT fusion reactions require not only suitable instrumentation but also an appropriate mechanism for charge exchange neutralization of such ions. For passive NPA measurements in the MeV range, the neutral flux is produced mainly by H^+, D^+, T^+ ions undergoing electron capture from hydrogen-like low-Z impurity ions [87]. In the case of He^{2+} ions, neutralization in the MeV range occurs by double electron capture from helium-like low-Z impurity ions [88]. The most probable donors for electron capture in large plasma machines like JET are carbon and beryllium ions because they are the main low-Z impurities in these machines and their densities in the plasma core are higher than the density of H^0.

In cases where NPA sightlines intersect energetic neutral beams, active charge exchange measurements are possible. For example, MeV ion measurements using 80 keV $^3He^o$ and 90 keV D^o neutral beams were performed on JT-60U [63] using the high energy Gemma-2 [60] NPA. However, fortuitous combinations of NPA sightlines and

neutral beams do not always exist and other charge exchange processes have been devised.

The active Pellet Charge Exchange (PCX) method [89] on TFTR [90, 91] using either Lithium or Boron pellets and the passive Impurity Ion Neutralization (IIN) method [92] on JT-60U [93], JET [94] and TFTR [95, 96] were used to measure energetic ions in the MeV energy range with the use of the Gemma-2 NPA. For Lithium pellets in the PCX method, H^+ and He^{2+} ions interacted with the pellet ablation cloud of Li^+ to form an equilibrium neutral fraction, $F_0(E)$, as a result of the reactions $H^+ + Li^+ \Rightarrow H + Li^{2+}$ and $^4He^{2+} + Li^+ = {}^4He + Li^{3+}$. A schematic illustrating the PCX concept is presented in Fig. 25. The $F_0(E)$ dependence on the alpha particle energy [91] is shown in Fig. 26. In the case of PCX measurements, the neutral flux generated in the plasma can be expressed as:

$$\phi_{SH,He}{}^{PCX}(E) = n_{H,He} f_{H,He}\left(F_0(E) \cdot V_{H,He}\right) \qquad (9)$$

where $n_{H,He}$ and $f_{H,He}$ are the density and distribution function of H^+ and He^{2+} ions, respectively, and $V_{H,He}$ is the ion velocity.

An example of the PCX measurement is shown in Fig. 27 where the evolution of the measured alpha energy spectra during the slowing-down phase and near the birth phase is compared with spectra computed using the FPPT code [97]. With the PCX method, a photodiode array orthogonal to the pellet path measured the position of the pellet in time to enable radially resolved measurements of energy spectra and density profiles of the confined energetic particles. This was exploited to measure the effects on the alpha particle distribution of classical slowing down, stochastic ripple diffusion, magnetic shear, α-TAE resonance and sawtooth activity [61] as well the radial profile of ICRF heated tritium ions [95, 96].

8. Neutron and Gamma Radiation Effects

High levels of neutron and neutron-induced gamma-ray fluxes during both DD and particularly DT operation of TFTR and JET have been a source of high-level noise counts for many diagnostics. On TFTR, typical source strengths were ~ $2x10^{16}$ n/s for 2.45 MeV neutrons during DD operation and ~ $2x10^{18}$ n/s during DT operations with roughly equivalent γ-ray yields in the respective cases. During TFTR experiments involving D-T discharges, the 14 MeV neutron flux levels in the environment of the MCP detector reach ~10^{11} neutrons/cm^2/s. An investigation of the neutron response of the MCP showed measured neutron detection efficiencies of $1.7x10^{-3}$ and $6.4x10^{-3}$ counts/neutron for 2.5 MeV-DD and 14 MeV-DT neutrons, respectively [98]. A shield to suppress neutron and gamma induced noise in the MCP was designed and implemented which consisted of 10-cm-thick inner housing of lead surrounded by a 23-cm-thick layer of 1.0% borated polyethylene. This shielding provided a measured reduction of 140x in the MCP noise level relative to an unshielded analyzer [99].

Aside from shielding, a correction for the residual neutron and gamma induced noise signal is facilitated on the TFTR-style EIIB analyzers by using a thin foil mask over detectors at the extreme ends of each mass row. The masked detectors respond only to the neutron and gamma radiation so that the noise levels were monitored as a function of time during the discharge to provide a time dependent correction for noise on the raw charge exchange signals.

Another approach developed for real-time neutron and gamma noise correction on the MAST EIIB diagnostic employs modulation (or gating) of the electrostatic field [100]. The gating technique that uses a fast push-pull high voltage transistor switch to modulate the voltage applied to the electrostatic deflection plates was devised primarily to reduce the dead time loss of the MCP detector thus extending the count range ceiling. As an additional benefit, during the electrostatic field off periods ions do not impinge on the MCP so only the neutron and gamma background noise is registered.

Thus the off-period signals can be used to provide real-time correction for the neutron and gamma background noise for the on-period signals.

Pulse height analysis of the detector signal offers another technique for discrimination against neutron and γ-ray noise since the neutron and γ-ray pulses are smaller than those generated by ions. For detectors using CsI(Tl) scintillators, the signal-to-noise ratio can be further enhanced by reducing the scintillator thickness to the minimum value required to fully stop the incident ion at the energy to be detected [63] combined when needed with supplemental secondary ion acceleration in the energy range of ~10 – 100 keV to enhance discrimination between lower energy ions and the neutron/γ-ray background [64].

Coincidence measurements as applied in the high-energy TOF analyzers [81-86] presented in Sec. 6 are another possibility to reduce the sensitivity of the system to neutrons and γ-rays. The neutrons and γ-rays do not result in secondary electrons emitted from the start foil, and morever, their efficiency for direct detection by the channeltron or channelplate detectors is small compared to that of the neutral particles from the plasma. These two effects give a strong reduction of the number of random coincidences by background neutrons and γ-rays.

Acknowledgments

Work supported by U. S. DoE Contract No. DE-AC02-76-CH03073. The work of of AD has been performed under the Association contract Euratom-FOM, with financial support from NWO and Euratom.

References

[1] V. V. Afrosimov, I.P. Gladkovskij I.F. Kalinkevich et al., “The Studies of Atomic Flux Emitted by Plasma,” Nuclear Fusion, Suppl. 1962, part 3, page 921

[2] L. F. Artsimovich, V. V. Afrosimov, I. P. Gladkovskij et al., “Ohmic Heating of the Plasma in Toroidal Machine Tokamak-3,” Plasma Physics and Controlled Nuclear Fusion Research, IAEA, Vienna, 1966, Vol. II, page 595

[3] I. A. Artsimovich, A .V. Glukhov, E .P. Gorbunov, M. P. Petrov, “The Energy Balance and the Lifetime of Ions in Plasma of Tokamak T-3,” IV European Conf. on Controlled Fusion and Plasma Physics, Rome, 1970, page 18

[4] Equipe TFR, "Tokamak Plasma Diagnostics," Nucl. Fusion 18, 647 (1978)

[5] N. C. Luhmann, Jr. and W. A. Peebles, "Instrumentation for Magnetically Confined Fusion Plasma Diagnostics," Rev. Sci. Instrum. **55**, 279 (1984)

[6] H. Hutchinson, *Principles of Plasma Diagnostics*, Cambridge University Press, Cambridge (1987) p. 284

[7] C. W. Barnes, *et al.*, *Diagnostics for Experimental Fusion Rectors, Plenum, New York, (1996)*

[8] C. B. Wharton, "A Review of Energetic Neutral Particle Plasma Diagnostics," Proc. 1st Course on Diagnostics and Data Acquisition Systems, Varenna, Italy (1975), p. 70

[9] F. Wagner, “Neutral Particle Diagnostics for Ohmically and Auxiliary Heated Tokamaks,” J. Vac. Sci. Technol. **20**,1211 (1982)

[10] W. W. Heidbrink and G. J. Sadler, “The Behaviour of Fast Ions in Tokamak Experiments,” Nucl. Fusion **34**, 535 (1994)

[11] S. Sudo, *et al.*, “Overview of Large Helical Device Diagnostics (invited),” Rev. Sci. Instrum. **72**, 483 (2001)

[12] A. C. Maas, *et al.*, “Diagnostic Experience during Deuterium-tritium Experiments in JET, Techniques and Measurements,” Fus. Eng. Design **47**, 247 (1999)

[13] S. L. Davis, D. Mueller and C. J. Keane, "Mass Resolving Charge-exchange System on the Poloidal Divertor Experiment," Rev. Sci. Instrum. **54**, 315 (1983)

[14] A. Nudelman, R. Goldston and R. Kaita, "The Fast Ion Diagnostic Neutral Beam Injector on the Poloidal Divertor Experiment," J. Vac. Sci. Technol. **20**,1284 (1982)

[15] S. S. Medley, "Simulation of the Diagnostic Neutral Beam for Active Charge-exchange Measurements on the Tokamak Fusion Test Reactor," Fusion Tech. **11**, 346(1987)

[16] G. Schilling, T. A. Kozum, S. S. Medley and K. M. Young, "TFTR Diagnostic Neutral Beam," Rev. Sci. Instrum. **57**, 2060 (1986)

[17] W. L. Rowan, *et al.*, "Neutral Beam Diagnostics for Alcator C-Mod," Rev. Sci. Instrum. **68**, 300 (1997)

[18] K. J. McCarthy, *et al.*, "Diagnostic Neutral Beam Injector and Associated Diagnostics Systems for the TJ-II Stellarator Device," Rev. Sci. Instrum. **75**, 3499 (2004)

[19] L. Q. Hu, *et al.*, "Neutral Beam Diagnostics for the HT-7 Tokamak," Rev. Sci. Instrum. **75**, 3496 (2004)

[20] P. Beiersdorfer, A. L. Roquemore and R.Kaita, "Characteristics of Compact Solid-target Charge Exchange Analyzers for Energetic Ion Diagnostics on Tokamaks," Rev. Sci. Instrum. **58**, 2092 (1987)

[21] V.Kh. Liechtenstein, T. M. Ivkova, E. D. Olshanski, et.al., "Recent investigations and applications of thin diamond-like carbon (DLC) foils," Nucl. Instr. and Meth. A 521 (2004) 197-202

[22] R. Kaita, R. J. Goldston, D. Meyerhofer and J. Eridon, "Design and Calibration of the Fast Ion Diagnostic Experiment Detector on the Poloidal Divertor Experiment," Rev. Sci. Instrum. **52**, 1795 (1981)

[23] R. J. Goldston, "Diagnostics for Hot Plasmas using Hydrogen Neutral Beams," Proc. Course Diagnostics for Fusion Reactor Conditions, Varenna, Italy (1982), p. 263

[24] E. M. Carolipio and W. W. Heidbrink, "Array of Neutral Particle Analyzers at DIII-D," Rev. Sci. Instrum. **68**, 304 (1997)

[25] H. J. Leisenfelder, R. L. Hancock, J. H. Resnick, T. P. Crowley and J. G. Schatz, “Electrostatic Energy Analyzer for Multi-MeV Heavy Ion Beam Probes,” Rev. Sci. Instrum. **63**, 4579 (1997)

[26] A. Fujisawa and Y. Hamada, “Theoretical Study of Cylindrical Energy Analyzers for MeV Range Heavy-ion Beam Probes,” Rev. Sci. Instrum. **64**, 3503 (1993)

[27] L. R. Boedeker, “Scanning Multiple Collector Electrostatic Analyzer with Application to Plasma Potential Measurement,” Rev. Sci. Instrum. **50**, 722 (1979)

[28] T. S. Green and G. A. Proca, “A Parallel Plate Electrostatic Spectrograph,” Rev. Sci. Instrum. **41**, 1409 (1970)

[29] A. W. Molvik, “Large Acceptance Angle Retarding-potential Analyzers,” Rev. Sci. Instrum. **52**, 704 (1981)

[30] K. McGuire, *et al.*, “Study of High-Beta Magnetohydrodynamic Modes and Fast-Ion Losses in PDX,” Phys. Rev. Lett. **50**, 891 (1983)

[31] R. J. Goldston, R. Kaita, P. Beiersdorfer, G. Gammel, D. L. Herndon, D. C. McCune, and D. D. Meyerhofer, "Charge Exchange Measurements of MHD Activity During Neutral Beam Injection in the Princeton Large Torus and the Poloidal Divertor Experiment," Nucl. Fusion **27**, 921 (1987)

[32] D. D. Meyerhofer, R. J. Goldston, R. Kaita, A. Cavallo, B. Grek, D. Johnson, D. C. McCune, K. McGuire, and R. B. White, "Measurement of Current Penetration During PDX Discharge Startup," Nucl. Fusion **25**, 321 (1985)

[33] V. V. Afrosimov, E. L. Berezovskii, I. P. Gladkovskii, A. I. Kislyakov, M. P. Petrov and M. P. Sadovnikov, “Multichannel Energy and Mass Analyzer for Atomic Particles,” Sov. Phys.-Tech. Phys. **20**, 33 (1975)

[34] W. E. Nexsen, Jr., W. C. Turner and W. F. Cummins, “Multi-channel Neutral-particle Analyzer System,” Rev. Sci. Instrum. **50**, 1227 (1979)

[35] S. S. Medley and A. L. Roquemore, “Construction and Operation of Parallel Electric and Magnetic Field Spectrometers for Mass/Energy Resolved Multi-ion Charge Exchange Diagnostics on the Tokamak Fusion Test Reactor,” Rev. Sci. Instrum. **69**, 2651 (1998)

[36] J. L. Wiza, " Microchannel Plate Detectors," Nucl. Instrum. Methods **162**, 587 (1979)

[37] A. L. Roquemore, G. Gammel, G. W. Hammett, R. Kaita and S. S. Medley, "Application of an E ||B Spectrometer to PLT Charge Exchange Diagnostics," Rev. Sci. Instrum. **56,** 1120 (1985)

[38] G. W. Hammett, R. Kaita and J. R. Wilson, “Measurements of Energetic Helium-3 Minority Distributions During Ion Cyclotron Radio-Frequency Heating in the Princeton Large Torus,” Nucl. Fusion **28**, 2027 (1988)

[39] R. Kaita, *et al.*, "Charge-Exchange and Fusion Reaction Measurements During Compression Experiments with Neutral Beam Heating in the Tokamak Fusion Test Reactor," Nucl. Fusion **26**, 863 (1986)

[40] W. W. Heidbrink, *et al.*, “The Diffusion of Fast Ions in Ohmic TFTR Discharges,” Phys. Fluids B **3**, 3167 (1991)

[41] R. Kaita, R. B. White, A. W. Morris, E. D. Fredrickson, K. McGuire, S. S. Medley and S. D. Scott, “Mode-particle Resonances during Near-tangential Neutral Beam Injection in the Tokamak Fusion Test Reactor,” Phys. Fluids B **2**, 1584 (1990)

[42] C. L. Fiore, S. S. Medley, G. W. Hammett, R. Kaita, A. L. Roquemore and S. Scott, "Ion Temperature From Tangential Charge Exchange Neutral Analysis on the Tokamak Fusion Test Reactor," Nucl. Fusion **28**, 1315 (1988)

[43] M. R. Wade, R. J. Colchin, J. F. Lyon, R. N. Morris, C. E. Thomas and A. L. Roquemore, "ATF Neutral Particle Analysis System," Rev. Sci. Instrum. **61**, 3202 (1990)

[44] M. Osakabe, M. Takeiri, S. S. Medley, A. L. Roquemore and J. E. Lyon, “Energetic Neutral Particle Analysis on LHD Using a TFTR E||B Analyzer,” 42nd APS-DPP Conference, Quebec City, Canada, 23-27 October, 2000, #DP1.120

[45] S. S. Medley and A. L. Roquemore, “Neutral Particle Analyzer Diagnostic on the National Spherical Torus Experiment,” Rev. Sci. Instrum. **75**, 3625 (2004)

[46] M. R. Tournianski, R. J. Akers and P. G. Carolan, “Anisotropic Fast Neutral Particle Spectra in the MAST Spherical Tokamak,” Plasma Phys. Control. Fusion **47**, 671 (2005)

[47] J. H. Foote, G. W. Coutts, L. R. Pedrotti, L. Schlander and B. E. Wood, "EIIB End-Loss-Ion Analyzer for Tandem-Mirror Experiment-Upgrade," Rev. Sci. Instrum. **56**, 1117 (1985)

[48] S. S. Medley, R. E. Bell, M. P. Petrov, A. L. Roquemore and E. V. Suvorkin, "Initial Neutral Particle Analyzer Measurements of Ion Temperature in the National Spherical Torus Experiment," Rev. Sci. Instrum. **74**, 1896 (2003)

[49] A. L. Rosenberg, *et al.*, "Fast Ion Absorption of the High Harmonic Fast Wave in the National Spherical Torus Experiment," Phys. Plasmas **11**, 2441 (2004)

[50] S. S. Medley, *et al.*, "MHD-induced Energetic Ion Los during H-mode Discharges in the National Spherical Torus Experiment," Nucl. Fusion **44**, 1158 (2004)

[51] C. J. Armentrout, G. Bramson and R. Evanko, "E Parallel B Canted Detector Neutral-Particle Spectrometer," Rev. Sci. Instrum. **56**, 2101 (1985)

[52] Y. Kusama, *et al.*, "Neutral Particle Analyzer with Energy Range up to 4 MeV for both Alpha Particles and Protons," Fusion Eng. Des. **34-35**, 531 (1997)

[53] C. Kurz and C. L. Fiore, "Neutral Particle Diagnostics for Alcator C-MOD," Rev. Sci. Instrum. **61**, 3119 (1990)

[54] T. Fall, B Terreault, G. Abel, A. Boileau, A. Cote, H. Y. Guo and W. W. Zuzak, "Novel Isotope Exchange Scenarios: Investigation of Particle Recycling in the TdeV Tokamak," Plasma Phys. Control. Fusion **36**, 1763 (1994)

[55] K. Hayashi, K. Hashimoto, H. Yamoto, H. Takeuchi, Y. Miura, T. Nishitani, M. Shiho, and H. Maeda, "Charge Exchange Neutral Particle Mass and Energy Analyzer for the JT-60 Tokamak," Rev. Sci. Instrum. **56**, 359 (March, 1985)

[56] R. Bartiromo, G. Bracco, M. Brusati, G. Grosso, S. Mantovani, B. Tilia, and V. Zanza, "Design and Calibration of the JET Neutral Particle Analyzer," Rev. Sci. Instrum. **58**, 788 (1987)

[57] H. Takeuchi, T. Matsuda, Y. Miura, M. Makoto, H. Maeda, K. Hashimoto and K. Hayashi, "Multi-Channel Mass-Separated Neutral Particle Energy Analyser for Simultaneous Measurements of Hydrogen and Deuterium Atoms Emitted from Tokamak Plasma," Jap. J. Appl. Phys. **22**, 1709 (1983)

[58] W. Hermann, *et al.*, “Diagnostic Method for Radial Electric Fields in Tokamaks by the Observationof Ripple-trapped Ions,” Rev. Sci. Instrum. **69**, 3165 (1998)

[59] A. Romannikov, *et al.*, “Measurement of Central Toroidal Rotation in Ohmic Tore Supra Plasmas,” Nucl. Fusion **40**, 319 (2000)

[60] A. I. Kislyakov, A. V. Khudoleev, S. S. Kozlovskij and M. P. Petrov, “High Energy Neutral Particle Analyzer,” Fusion Eng. Des. **34-35**, 107 (1997)

[61] S. S. Medley, *et al.*, “Confined Trapped Alpha Behaviour in TFTR Deuterium-tritium Plasmas,” Nucl. Fusion **38**, 1283 (1998)

[62] A. A. Korotkov, A. Gondhalekar, and R. J. Akers, “Observation of MeV Energy Deuterons Produced by Knock-on Collisions between Deuterium-tritium Fusion a-particles and Plasma Fuel Ions,” Phys. Plasmas **7**, 957 (2000)

[63] Y. Kusama, *et al.*, “Charge-exchange Neutral Particle Measurement in MeV Energy Range on JT-60U,” Rev. Sci. Instrum. **66**, 339 (1995)

[64] V. I. Afanasyev, *et al.*, “Neutral Particle Analyzer/Isotope Separator for Measurement of Hydrogen Isotope Composition of JET Plasmas,” Rev. Sci. Instrum. **74**, 2338 (2003)

[65] M. Mironov, V. Afanasyev, A. Murari, et al., “Tritium Transport Studies with JET ISEP NPA During the Trace Tritium Experimental Campaign”31-th EPS Conference on Controlled Fusion and Plasma Physics, London, June, 2004

[66] F. V. Chernyshev V. I. Afanasyev A. V. Dech et al., “A Compact Neutral-Particle Analyzer for Plasma Diagnostics,“ Instruments and Experimental Techniques, Vol. 47, No. 2, 2004, pp. 214–220. Translated from Pribory i Tekhnika Eksperimenta, No. 2, 2004, pp. 87–93.

[67] D. E. Voss and S. A. Cohen, “Low Energy Neutral Outflux from the PLT Tokamak,” J. Nucl. Mater. **93/94**, 405 (1980)

[68] H. Verbeek, “A Low-energy Neutral Particle Analyser for Plasma Experiments,” J. Phys. E **19**, 964 (1986)

[69] H. Verbeek, *et al.,* "The Particle Fluxes in the Edge Plasma during Discharges with Improved Ohmic Confinement in ASDEX," Plasma Phys. Control. Fusion **32**, 651 (1990)

[70] Y. Miura and F. Okano, "Low-energy Neutral Particle Analysis by a Time-of-Flight Method on JFT-2M," Rev. Sci. Instrum. **61**, 3581 (1990)

[71] S. Costa *et al., "*The Time-of-Flight Neutral Particle Analyzer and its Calibration System for the RFX Experiment," Rev. Sci. Instrum. **66**, 330 (1995)

[72] S. Costa, A. Murari and L. Lotto, "First Results of Reverse Field Experiment Vertical Time-of-Flight," Rev. Sci. Instrum. **72**, 607 (2001)

[73] R. L. Boivin, M. Koltonyuk, C. P. Munson and R. M. Mayo, "Time-of-Flight Neutral Particle Analyzer for Alcator C-Mod," Rev. Sci. Instrum. **68**, 982 (1997)

[74] M. Ichimura *et al.,* "Measurement of Ion Temperature and Density Profiles with a Time-of-Flight Type Neutral Particle Analyzer," Rev. Sci. Instrum. **75**, 3637 (2004)

[75] W. van Toledo, A. R. de Bree, R. Van Buuren, H. De Kluiver and A. J. H. Donné, "A Time-of-Flight Spectrometer for Detection of Low-energy Hydrogen Atoms," Rev. Sci. Instrum. **61**, 622 (1990)

[76] W. van Toledo, R. Van Buuren, H. De Kluiver and A. J. H. Donné, "H^--conversion Aided Detection of Low Energy H^0 Fluxes from the TORTUR Tokamak in a Time-of-Flight Analyzer," Rev. Sci. Instrum. **63**, 2223 (1992)

[77] W. A. de Zeeuw, H. W. van der Ven, J. M. M. de Wit and A. J. H. Donné, "An Electrostatic Time-of-flight Analyzer for Simultaneous Energy and Mass Determination of Neutral Particles," Rev. Sci. Instrum. **62**, 110-117 (1991)

[78] G. Bracco, G. Betello, S. Mantovani, A. Moleti, B. Tilia, and V. Zanza, "Design and Calibration of the JET Time of Flight Neutral Particle Analyzer with High Noise Rejection Capability," Rev. Sci. Instrum. **63**, 5685 (1992)

[79] T. Ozaki, *et al.*, "High-energy Neutral Particle Measurement System in the Large Helical Device," Rev. Sci. Instrum. **71**, 2698 (2000)

[80] M. A. Gruntman and V .A. Morozov, "H Atom Detection and Energy Analysis by use of Thin Foils and TOF Technique," J. Phys. E **15**, 1356 (1982)

[81] A. J. H. Donné, E. P. Barbian and H. W. van der Ven, “On the Application of the Rutherford-scattering Diagnostics to Ion Temperature Measurements,” J. Appl. Phys. **62**, 3130 (1987)

[82] A. A. E. van Blokland, T. W. M. Grimbergen and H. W. van der Ven, “A Mass-selective Neutral Particle Energy Analyzer with Background Rejection,” Rev. Sci. Instrum. **63**, 1978 (1992)

[83] L. D. Horton *et al.,* J. Nucl. Mater. **196-198**, 139 (1992)

[84] T. Ozaki *et al.,* ”Design Study of High Energy Neutral Particle Measurements in a LHD,” Fusion Eng. Design **34-35**, 535 (1997)

[85] T. Ozaki *et al.,* “Spatial Resolved High-energy Particle Diagnostic System using Time-of-Flight Neutral Particle Analyzer in Large Helical Device,” Rev. Sci. Instrum. **74**, 1878 (2003)

[86] T. Ozaki *et al.,* ”Horizontal, Vertical and Radial High-energy Particle Distribution Measurement System in Large Helical Device,” Rev. Sci. Instrum. **77**, 10E917 (2006)

[87] M. P. Petrov *et al.*, “Neutral Particle Analysis in the MeV Range in JET,” *Proc. 1992 Int. Conf. on Plasma Physics,* Innsbruck, 1992, vol. 16C, Part II, p. II-1031.

[88] A. A. Korotkov and A. M. Ermolaev, “Impurity Induced Neutralization of Alpha-particles and Application to ITER Diagnostics,” *Proc. 22nd EPS Conf. on Controlled Fusion and Plasma Physics,* Bournemouth, 1995, Vol. 19C, Contributed Papers, Part III, European Physical Society, Geneva (1995) p.389.

[89] R. K. Fisher, *et al.*, “Alpha Particle Diagnostics using Impurity Pellet Injection (Invited),” Rev. Sci. Instrum. **63**, 4499 (1992)

[90] S. S. Medley, *et al.*, “Design and Operation of the Pellet Charge Exchange Diagnostic for Measurement of Energetic Confined α-Particles and Tritons on the Tokamak Fusion Test Reactor,” Rev. Sci. Instrum. **67**, 3122 (1996)

[91] S. S. Medley, *et al.*, “Measurements of Confined Alphas and Tritons in the MHD Quiescent Core of TFTR Plasma using the Pellet Charge Exchange Diagnostic,” Plasma Phys. Control. Fusion **38**, 1779 (1996)

[92] A. A. Korotkov, A. Gondhalekar and A. J. Stuart, “Impurity Induced Neutralization of Mega-electron-volt Energy Protons in JET Plasmas,” Nucl. Fusion **37**, 35 (1997)

[93] V. I. Afanassiev, *et al.*, “Neutral Particle Analysis in MeV Energy Range and Relative Role of He^{+} and C^{5+} Ions in Fast Proton Neutralization in ICRF and Combined ICRF/NBI-heated JT-60U Plasmas,” Plasma Phys. Control. Fusion **39**, 1509 (1997)

[94] S. E. Sharapov, *et al.*, “Energetic Particle Physics in JET,” Nucl. Fusion **40**, 1363 (2000)

[95] M. P. Petrov, *et al.*, “Effective Temperatures, Sawtooth Mixing and Stochastic Diffusion Ripple Loss of Fast H^{+} Minority Ions Driven by Ion Cyclotron Heating in the Tokamak Fusion Test Reactor,” Phys. Plasmas **6**, 957 (1999)

[96] H. H. Duong, *et al.*, “Radio Frequency-driven Energetic Tritium Ion Tail Measurements in the Tokamak Fusion Test Reactor using the Pellet Charge Exchange Diagnostic,” Rev. Sci. Instrum. **68**, 340 (1997)

[97] N. N. Gorelenkov, *et al.*, “Modelling of Alpha Particle Slowing Down, Confinement and Redistribution by Sawteeth in TFTR using the FPPT Code,” Nucl. Fusion **37**, 1053 (1997)

[98] S. S. Medley and R. Persing, "Response of a Chevron Microchannel Plate to 2.5 and 14 MeV Neutrons," Rev. Sci. Instrum. **52**, 1463 (1981)

[99] A. L. Roquemore, S. S. Medley, and S. D. Scott, "Design and Performance Characteristics of the Radiation Shield Developed for the TFTR Charge Exchange Diagnostics," Rev. Sci. Instrum. **59,** 1726 (1988)

[100] M. R. Tournianski, P. G. Carolan and R. J. Akers, “ Enhanced Microchannel Plate Performance at High Particle Fluxes by Pulsed Exposure Mode of Operation,” Rev. Sci. Instrum. **75,** 2854 (2004)

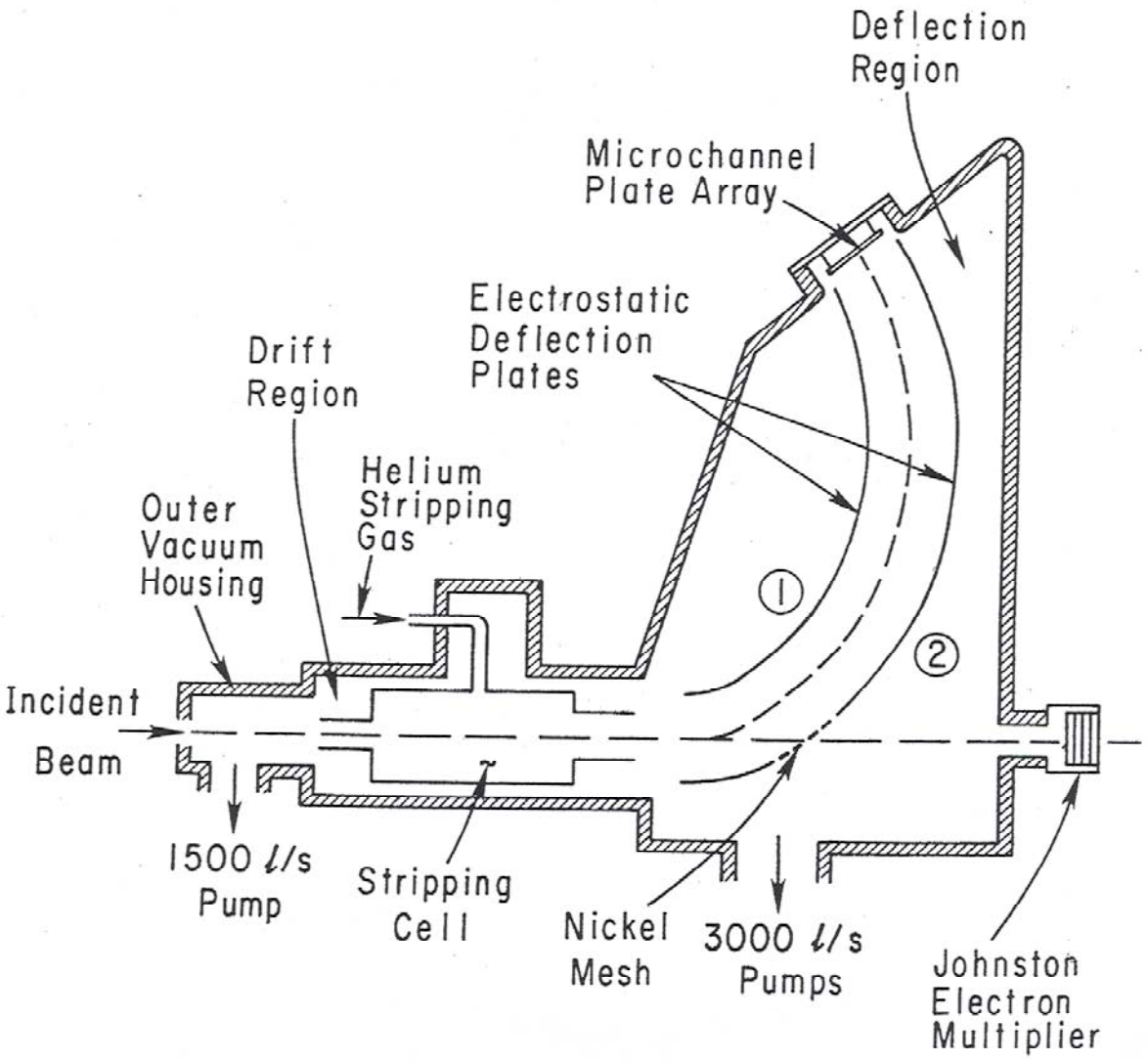

Fig. 1a. Schematic of the Fast Ion Diagnostic Experiment (FIDE) cylindrical plate electrostatic energy analyzer used on the Poloidal Divertor Experiment (PDX) depicting the relative positions of the stripping cell, the deflection plates, the MCP array and the Johnston electron multiplier. Deflection plate 1 (plate 2) is at negative (positive) potential [22].

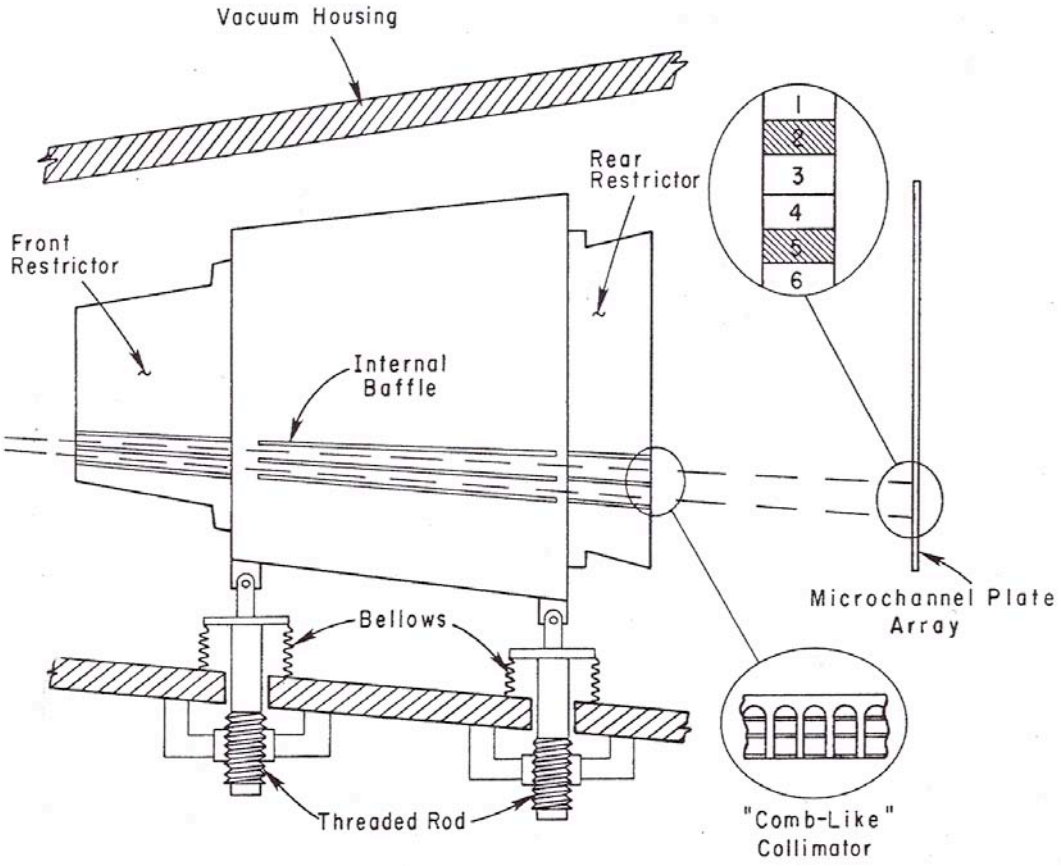

Fig. 1b. Schematic of the Fast Ion Diagnostic Experiment (FIDE) stripping cell and collimation mechanism. The geometry of internal baffles and the locations of the “comb-like” collimator are shown [22].

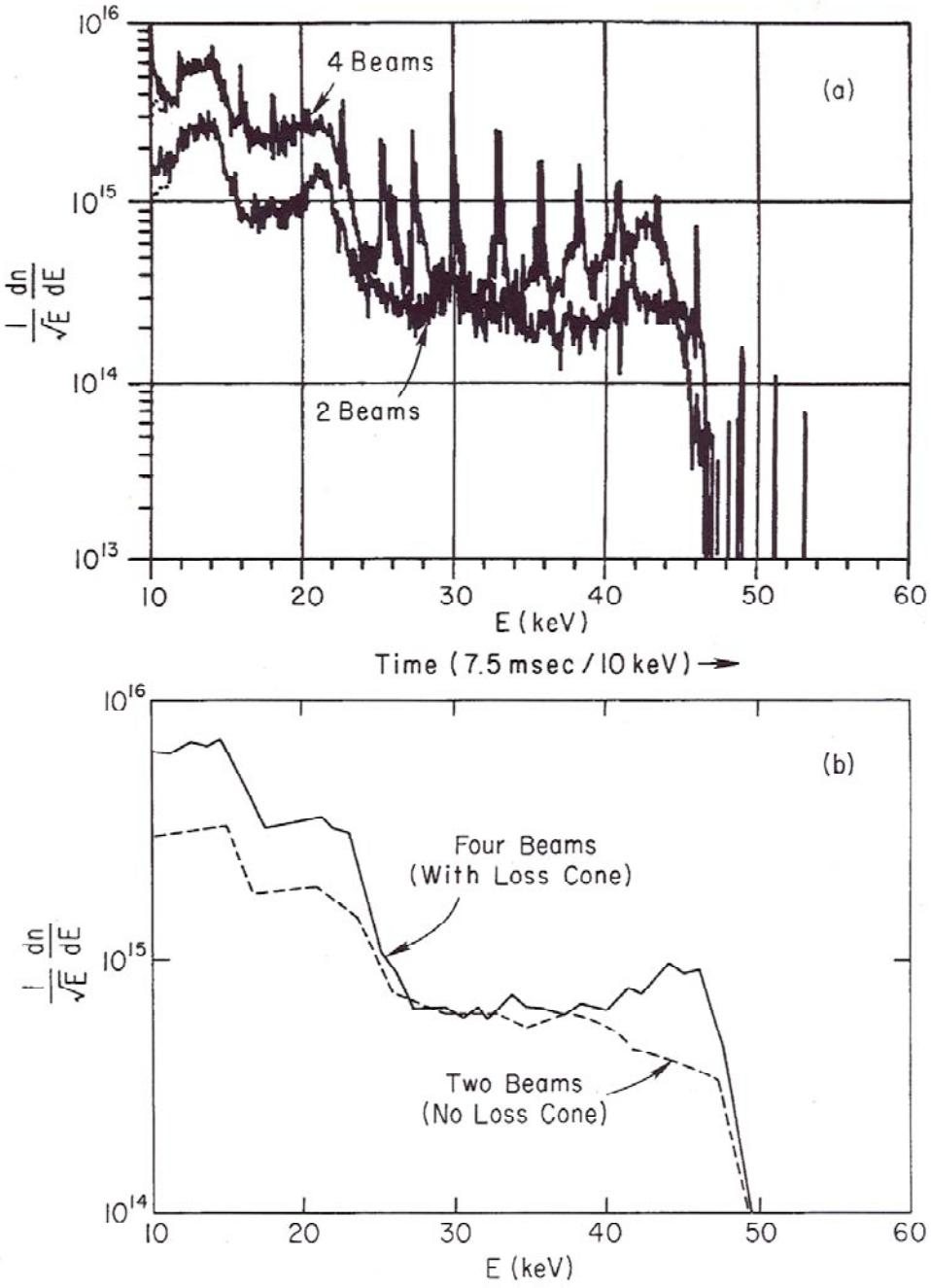

Fig. 2. The upper panel shows FIDE charge-exchange spectra from PDX for a no-fishbone discharge (2 beams) compared with a severe-fishbone discharge (4 beams). The depletion of beam ions in the region $E_{inj/2} < E < E_{inj}$ is evident (E_{inj} = 46 keV). Note that these spectra were obtained by sweeping the energy analyzer in time, so that fishbone spikes appear to be localized in energy but in fact they are localized in time. The lower panel shows simulations of the spectra using a bounce-averaged Fokker-Planck code [31].

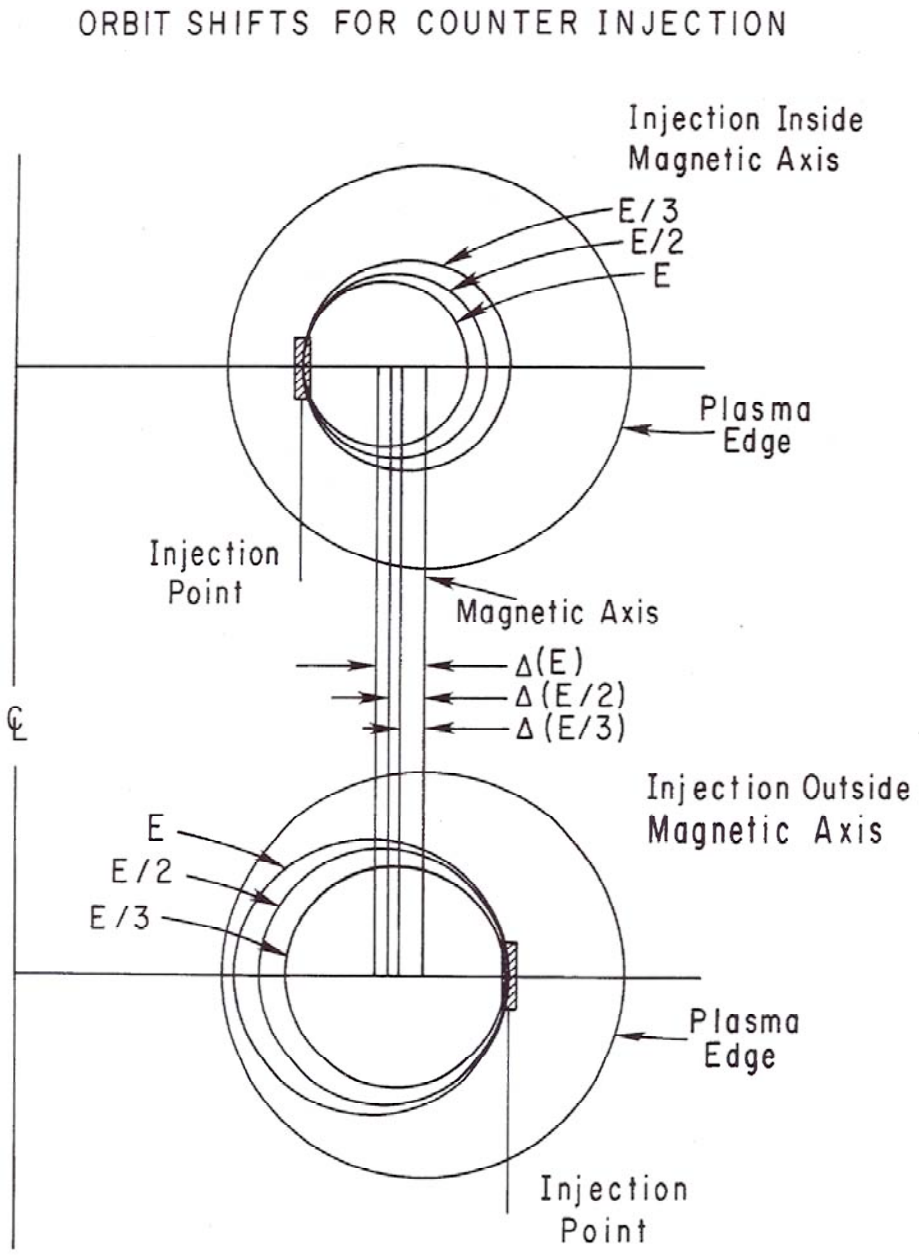

Fig. 3. Illustration of orbit shifts for counter-injection of the diagnostic neutral beam on PDX experiments to measure the q-profile using neutral particle diagnostics [32].

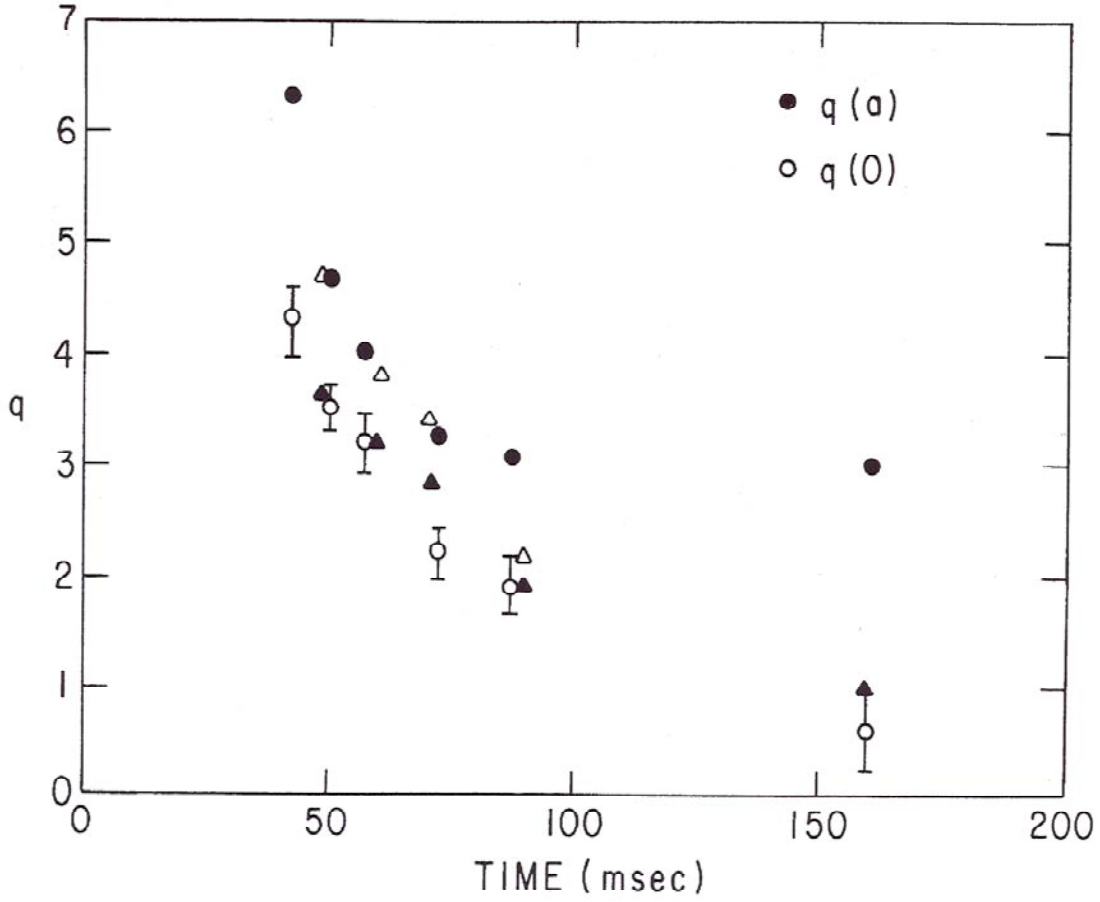

Fig. 4. Time evolution of q(a) and q measured near the plasma core, q(0), for PDX start-up obtained using neutral particle diagnostics [23].

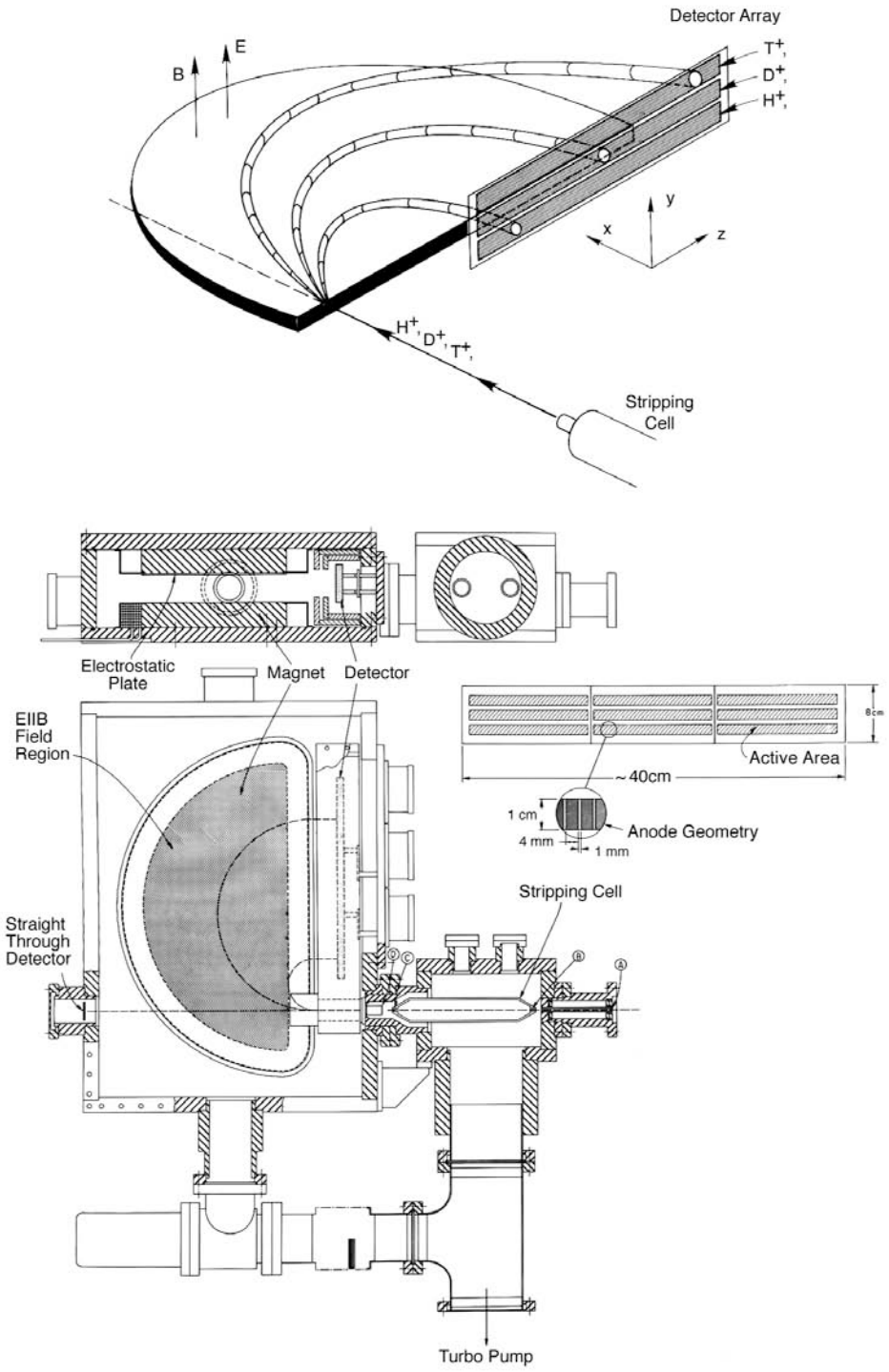

Fig. 5. Illustration of the EIIB concept (upper panel) and a schematic of the EIIB spectrometer design (bottom panel) showing plan and elevation cross-sections of the EIIB analyzer with the insert (not to scale) illustrating the geometry of the MCP detector [35].

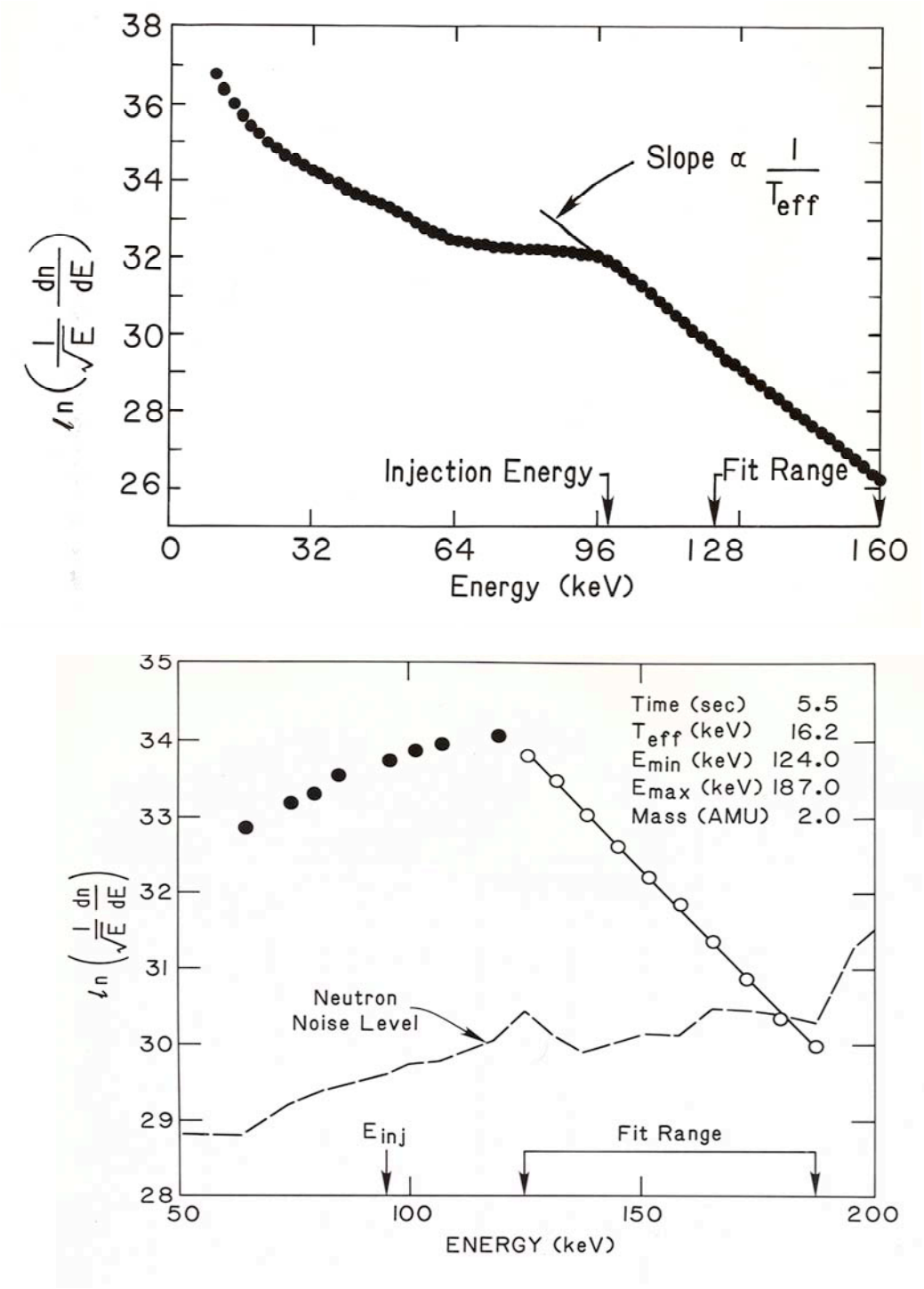

Fig. 6. The upper panel shows a Fokker-Planck calculation of the tangential deuterium NPA spectrum for a typical TFTR energetic ion mode discharge. The lower panel shows a deuterium charge exchange spectrum measured using the tangential EIIB NPA. A linear least-squares fit to the data in the energy range of E = 124 – 187 keV (open circles) yields T_{eff} = 16.2 keV [42].

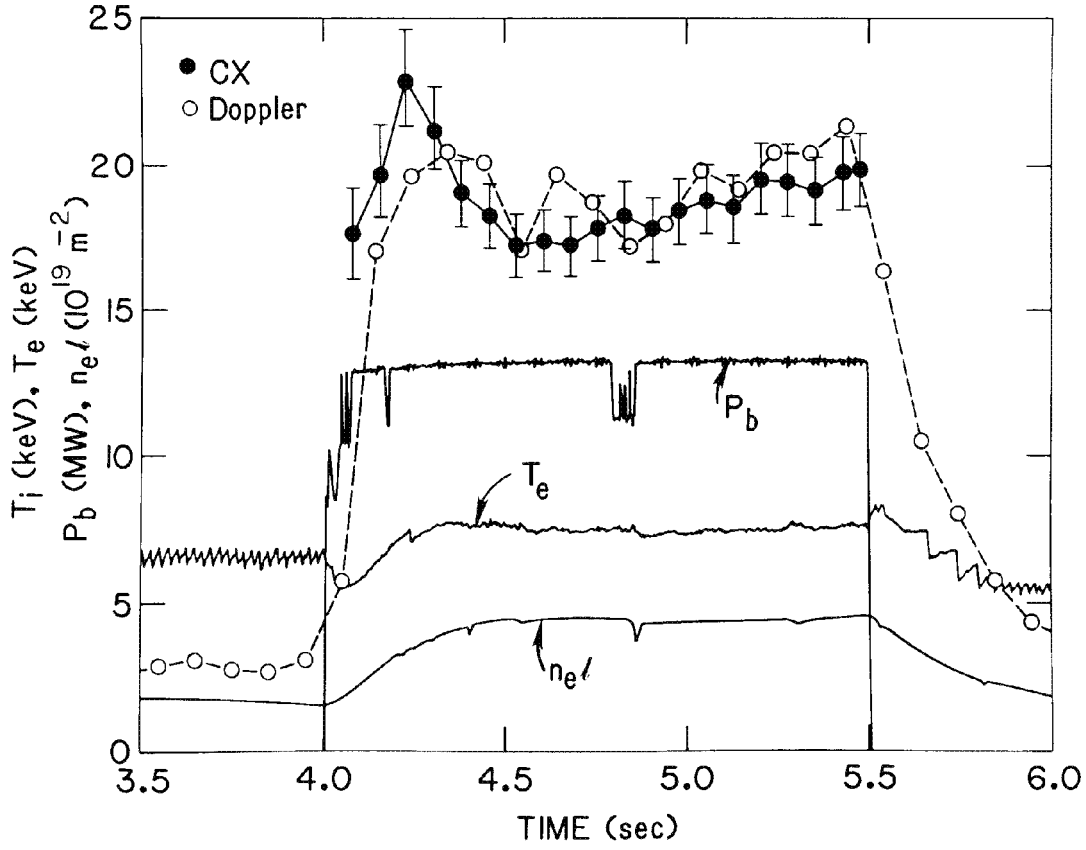

Fig. 7. Central ion temperature measured on TFTR using the tangential supra-beam charge exchange technique (solid circles) in comparison with measurements from the horizontal X-ray crystal diagnostic using the Doppler broadening of the Ni XXVII K_α impurity line emission (open circles) for a discharge with low toroidal rotation velocity ($v_\phi \leq 1.5 \times 10^5$ ms^{-1}). The toroidal rotation correction to the charge exchange data is small (< 7%) and has not been applied to this data [42].

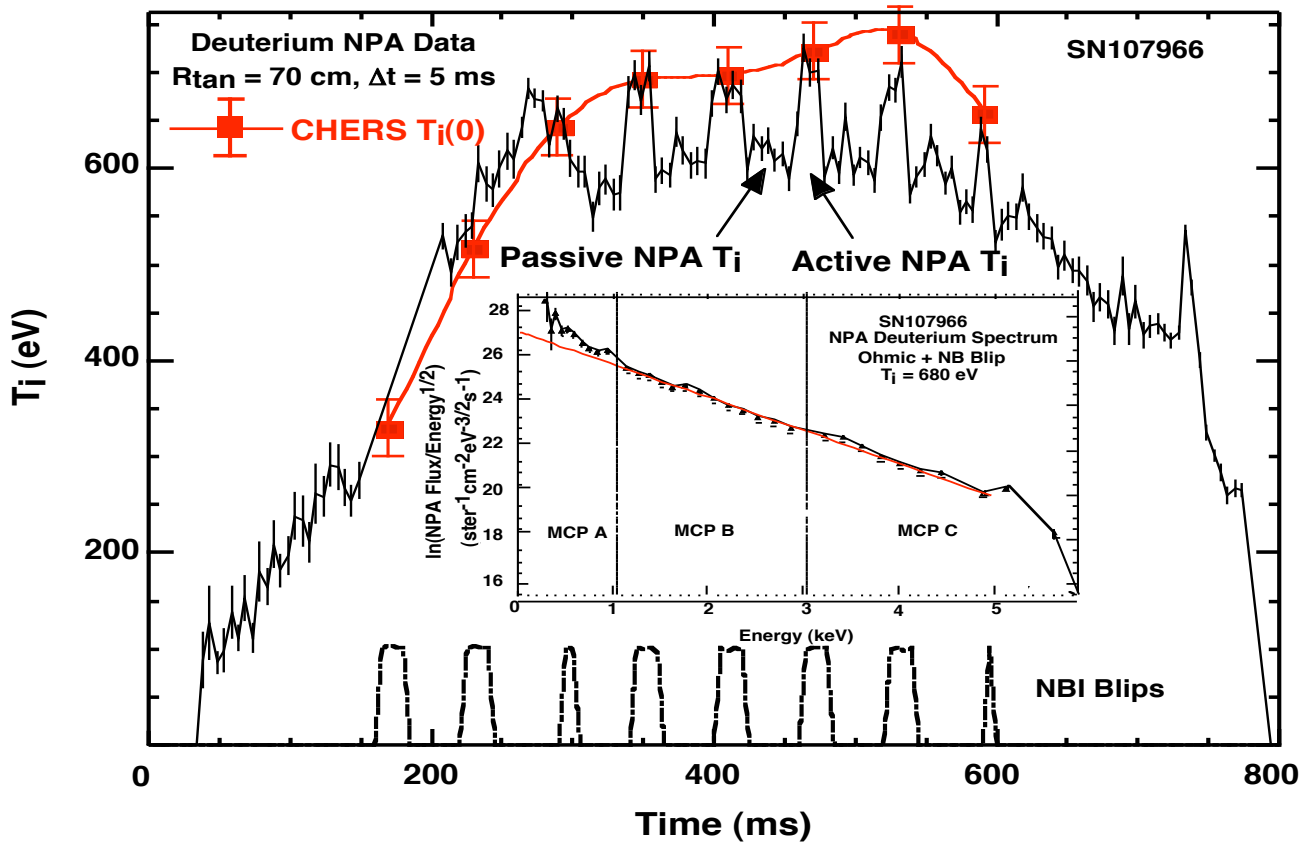

Fig. 8. Passive and active measurements of the deuterium ion temperature in an Ohmic discharge in NSTX using the EIIB neutral particle analyzer are shown. During the NB "blips" good agreement is observed between the NPA and CHERS measurements. A typical deuterium thermal spectrum is shown in the inset [45].

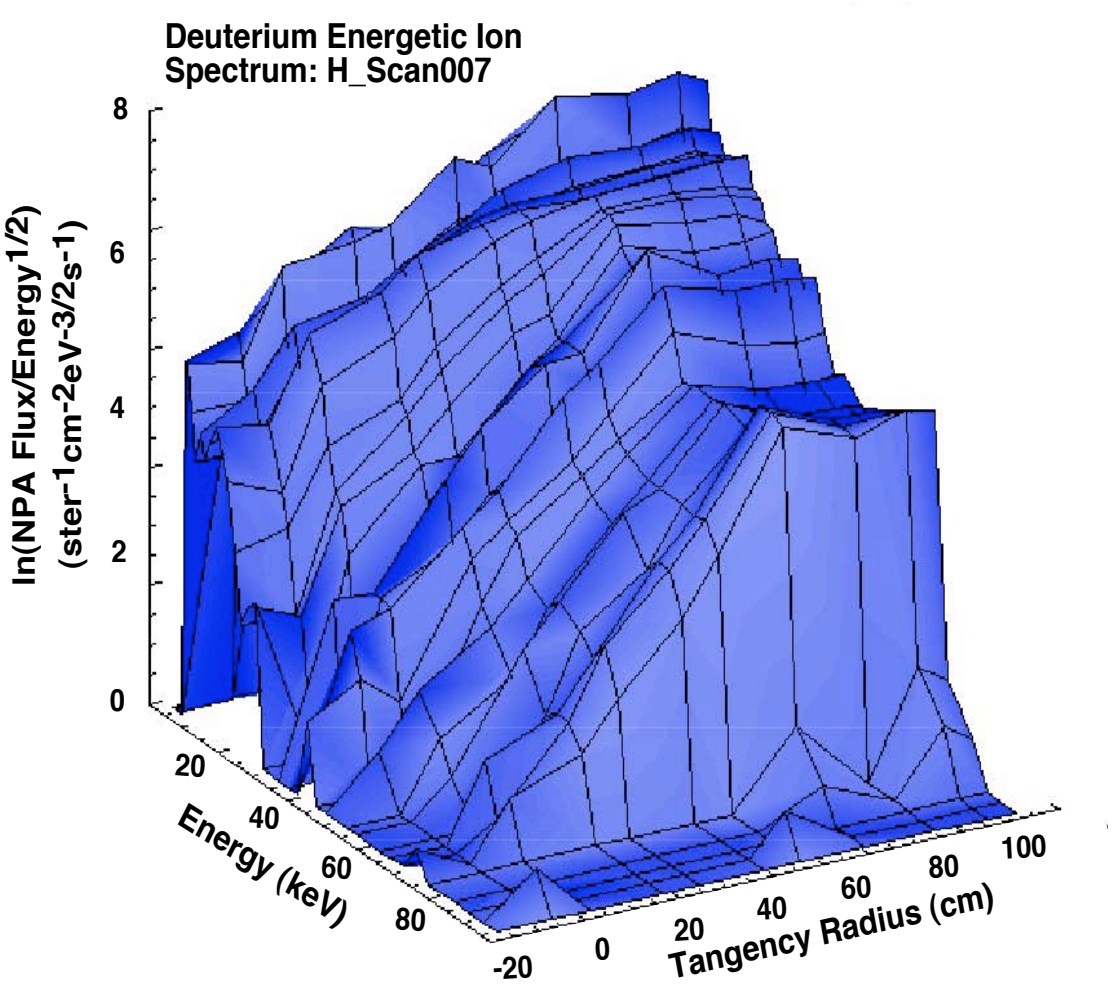

Fig. 9. Shown is the EIIB NPA measurement of the neutral beam ion distribution versus energy and tangency radius for source B injection on NSTX. The spectrum peaks around the beam injection tangency radius, R_{NB} = 59 cm, and is highly anisotropic [45].

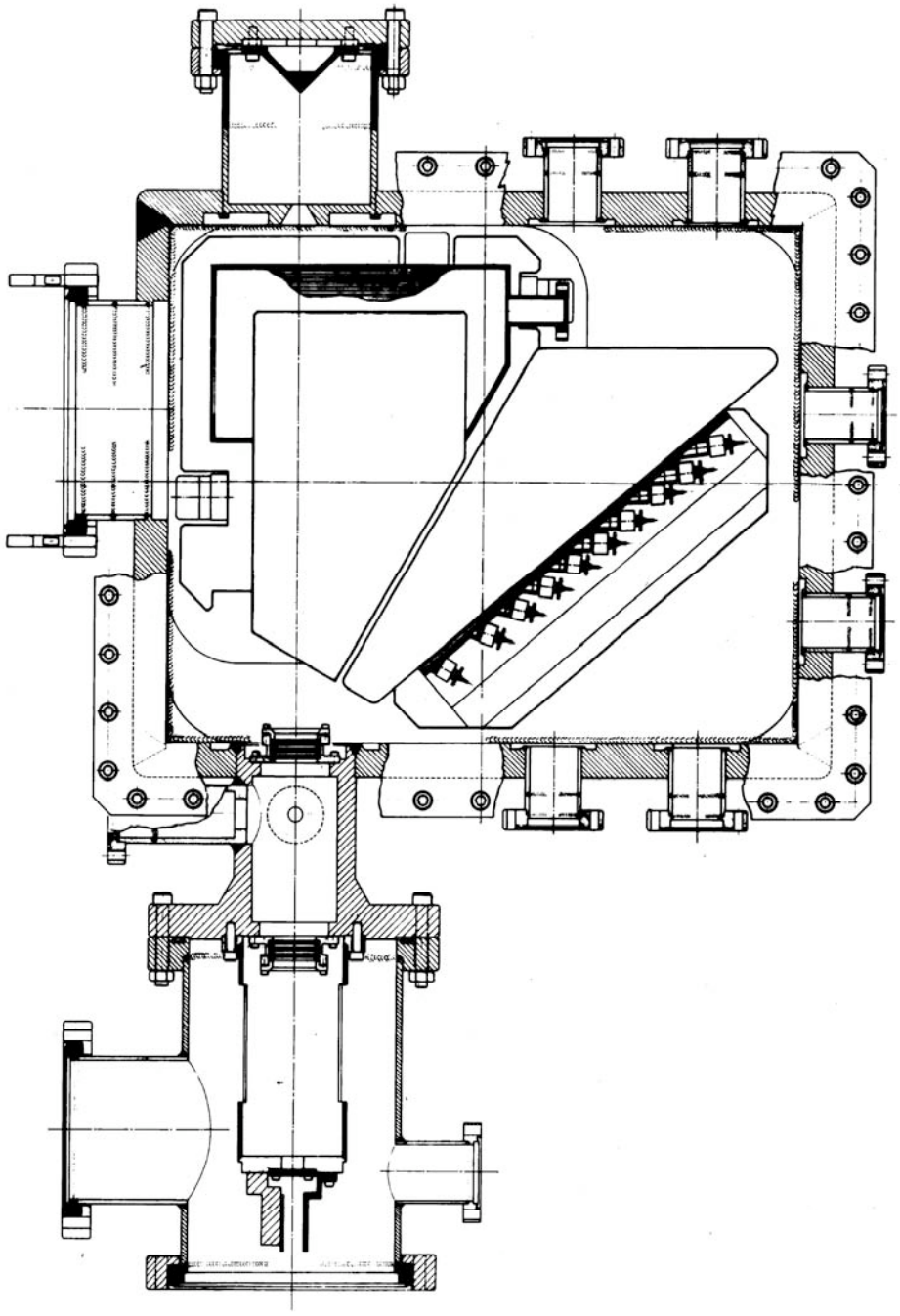

Fig. 10. The typical layout for a tandem EIIB type neutral particle analyzer is shown in plan (upper panel) and elevation (lower panel) views [53]. Charge exchange neutrals re-ionized in the stripping cell undergo momentum analysis in the magnetic sector followed by energy analysis in the tandem electrostatic plate sector. The channeltron detector plane exhibits linear rows of mass and energy resolved ions [56].

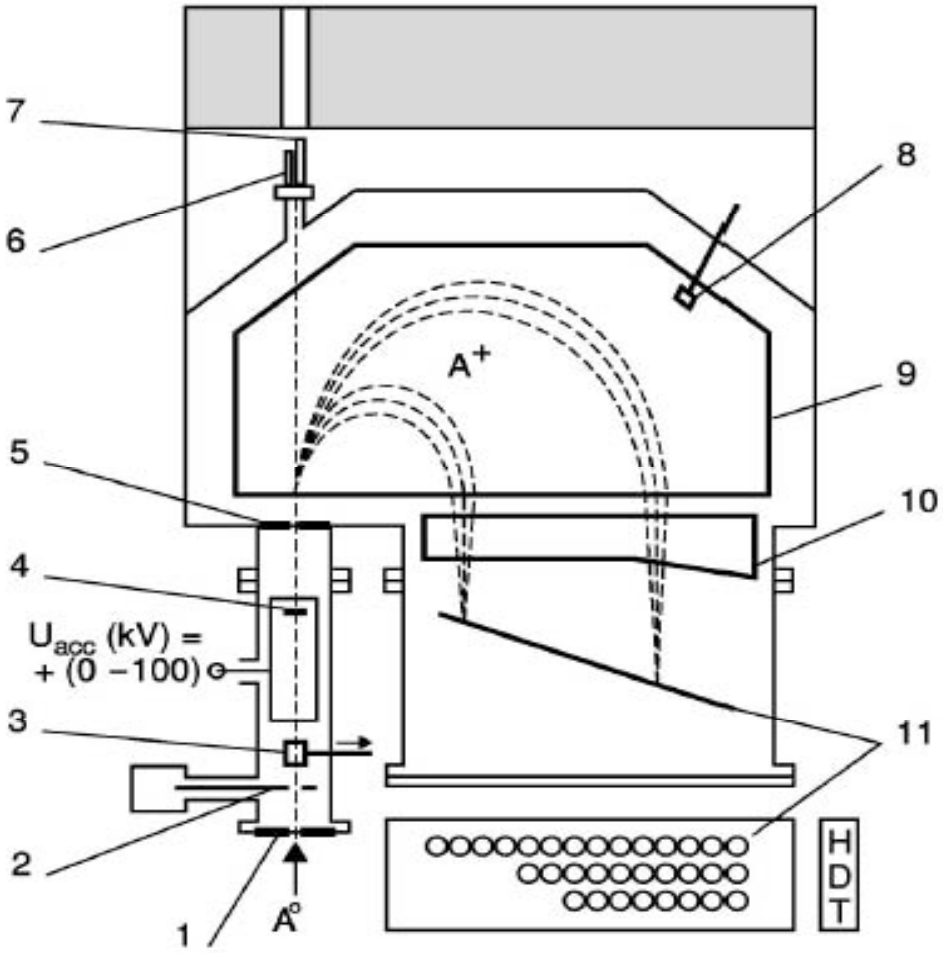

Fig. 11. ISEP NPA layout showing the elements of the instrument: 1 - input diaphragm, 2 - collimator slit mechanism, 3 - auxiliary movable calibration aid, 4 - stripping foil, 5 - output diaphragm, 6 - light emission diode, 7 - alignment laser, 8 - Hall probe, 9 - analyzing magnet, 10 - analyzing electrostatic condenser, 11 - detector array with 32 scintillator/PMT assemblies. A^0 is the atomic flux emitted by the plasma and A^+ is the reionized atomic flux [64].

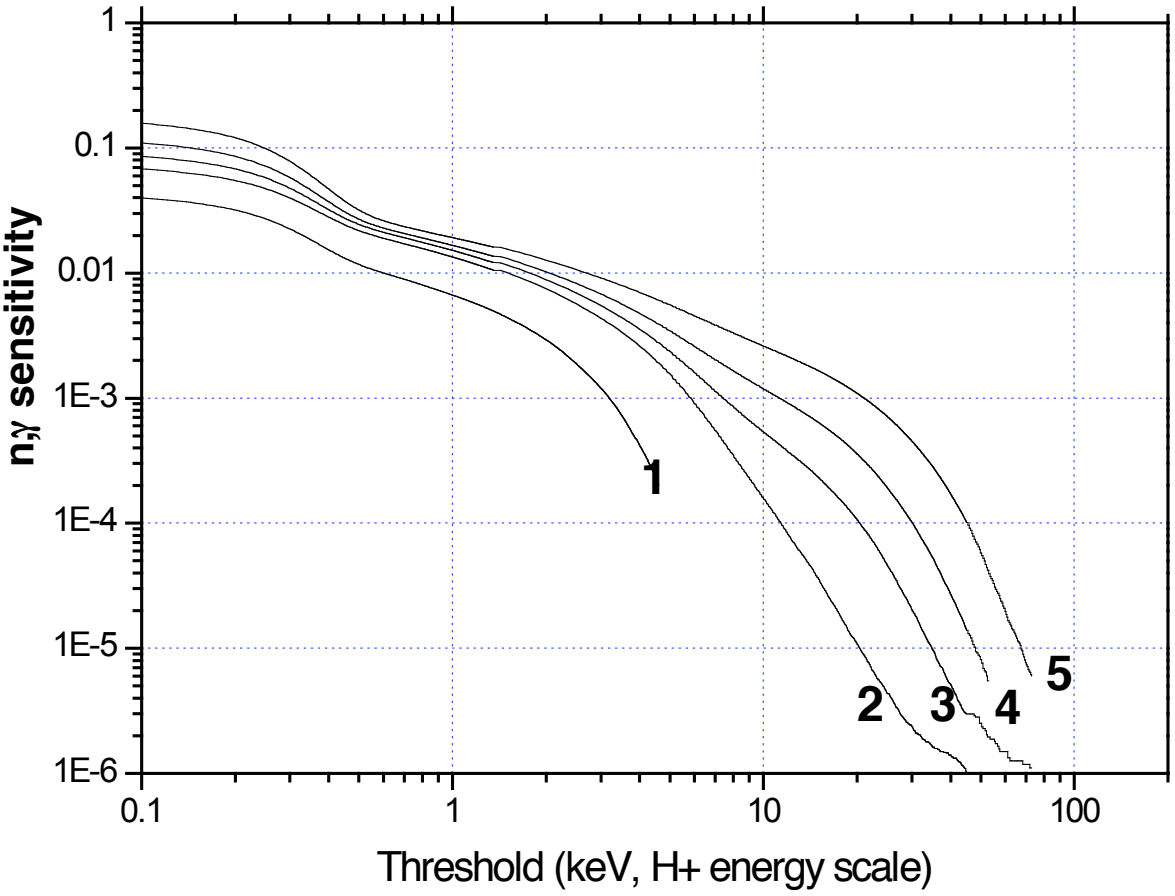

Fig. 12. Results of laboratory tests of the neutron and gamma sensitivity of the ISEP detector using a radioactive ^{252}Cf neutron source. Curve 1- bare PMT (without scintillator), curve 2 -1.1 μ scintillator (used in the lowest energy channels), curve 3 - 2.4 μ, curve 4 - 4.0 μ, curve 5 - 7.0 μ (used in the highest energy channel) [64].

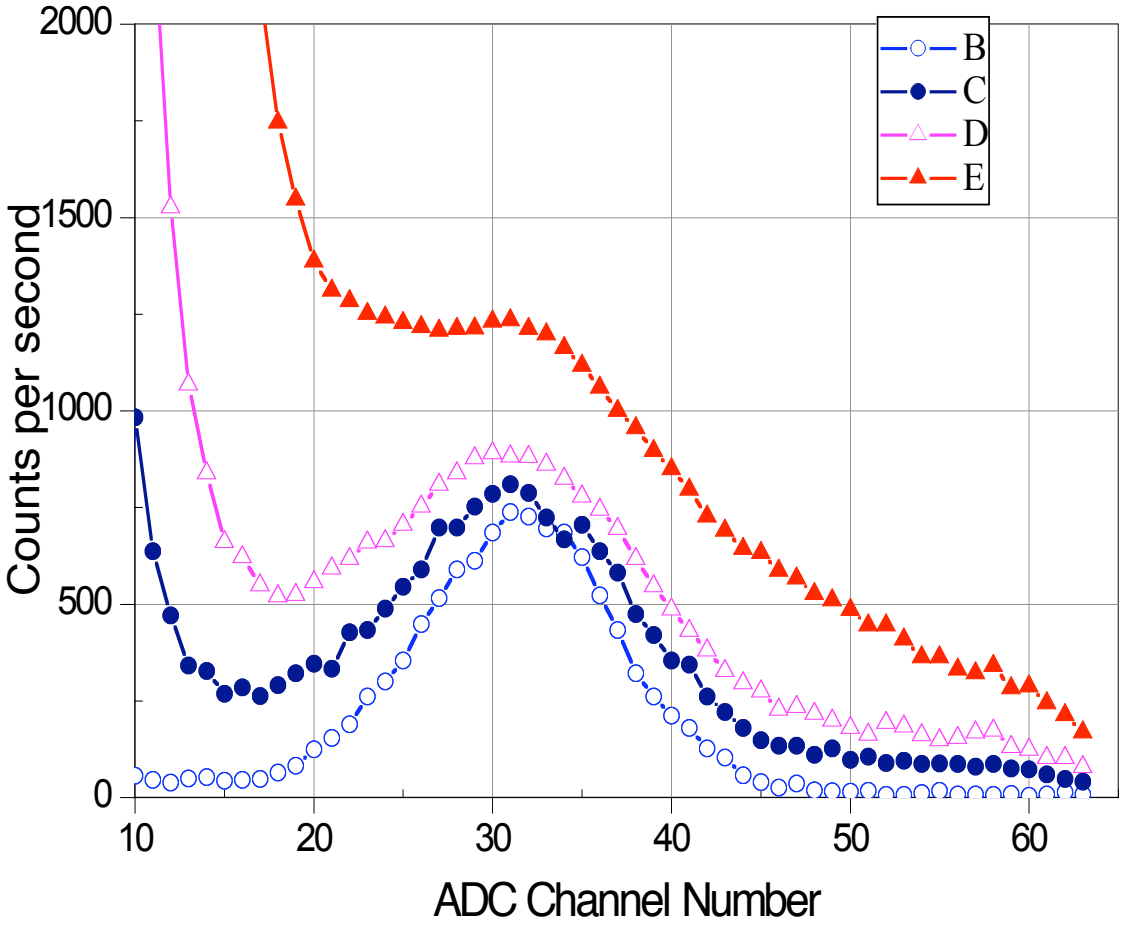

Fig. 13. Shown is a computer code simulation of the ISEP detector pulse height distribution for detection of D^+ ions in the presence of DT neutron radiation. The ion energy is $E_d = 5$ keV, acceleration voltage $U_{ac} = 80$ keV (total energy $E_D = 85$ keV), D^+ count rate is 10^4 s^{-1}. The neutron emission rate varies from 1×10^{17} n/s (curve B) to 5×10^{18} n/s (curve E) [64].

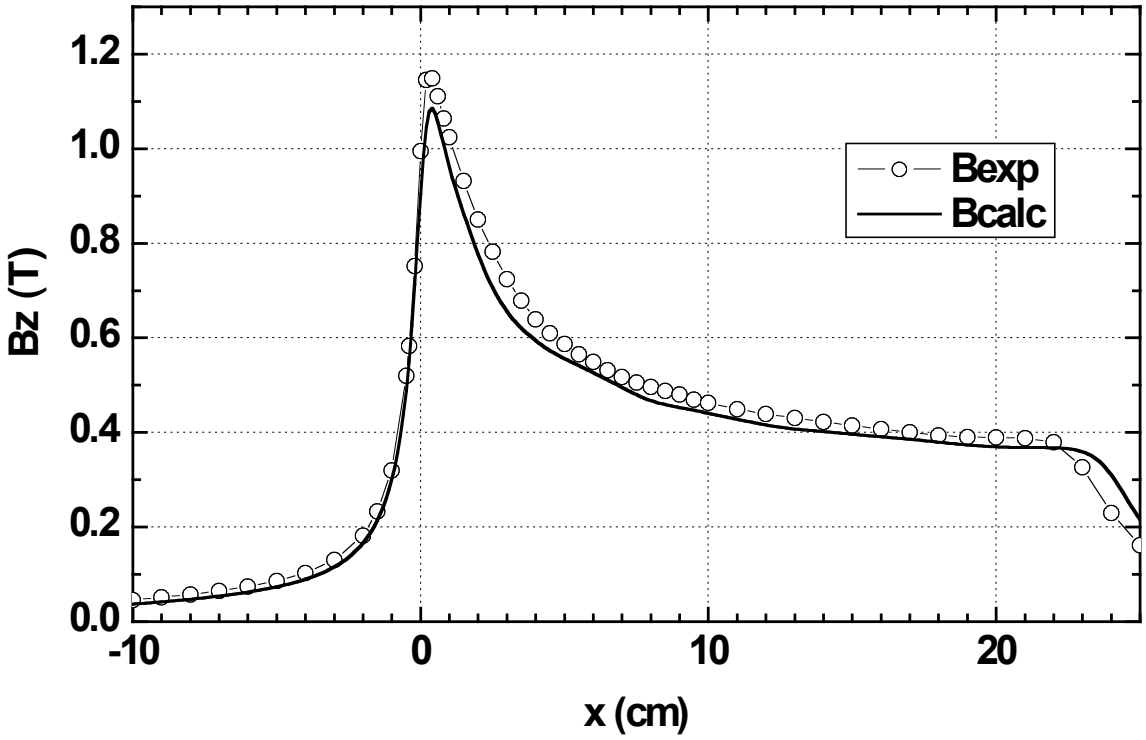

Fig. 14. The intensity of ISEP magnetic field versus distance from the entrance edge of the magnet is shown. The open circles are the experimental measurements made with the use of a Hall Probe and the solid line is the calculation [64].

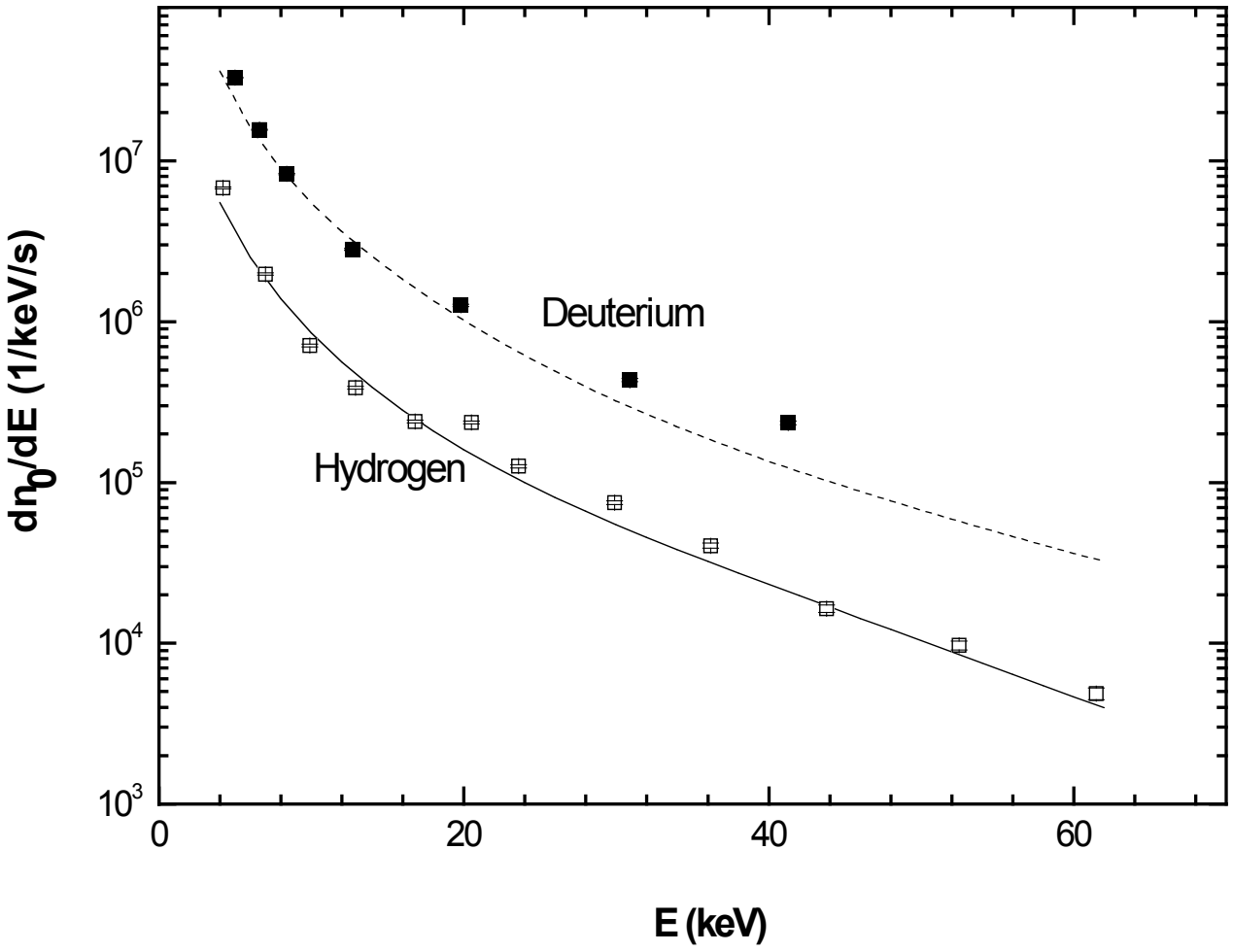

Fig. 15. Deuterium and hydrogen atom spectra for the case of a beam-heated high density JET plasma (shot #52246, 57.5 – 58.5 s, deuterium heating beams, total beam power = 12.6 MW) are shown. Solid and open symbols correspond to deuterium and hydrogen. Dashed and solid lines are the results of numerical modeling of atom energy spectra [64].

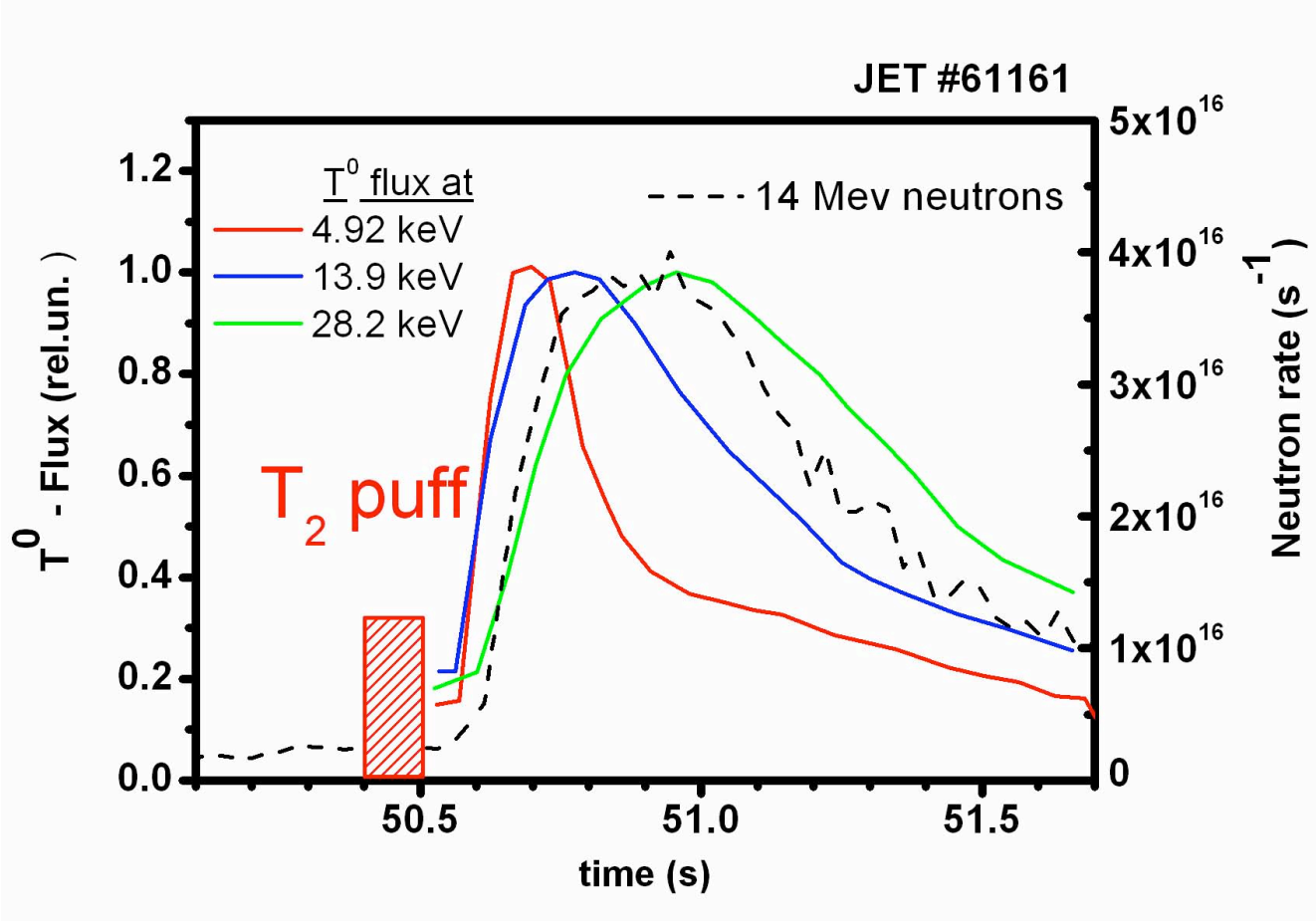

Fig. 16 Shown are typical time evolutions of tritium neutral fluxes with different energies detected by ISEP in a JET trace tritium experiment (shot #61161) with T_2 gas puff along with the intensity of 14 MeV neutrons [65].

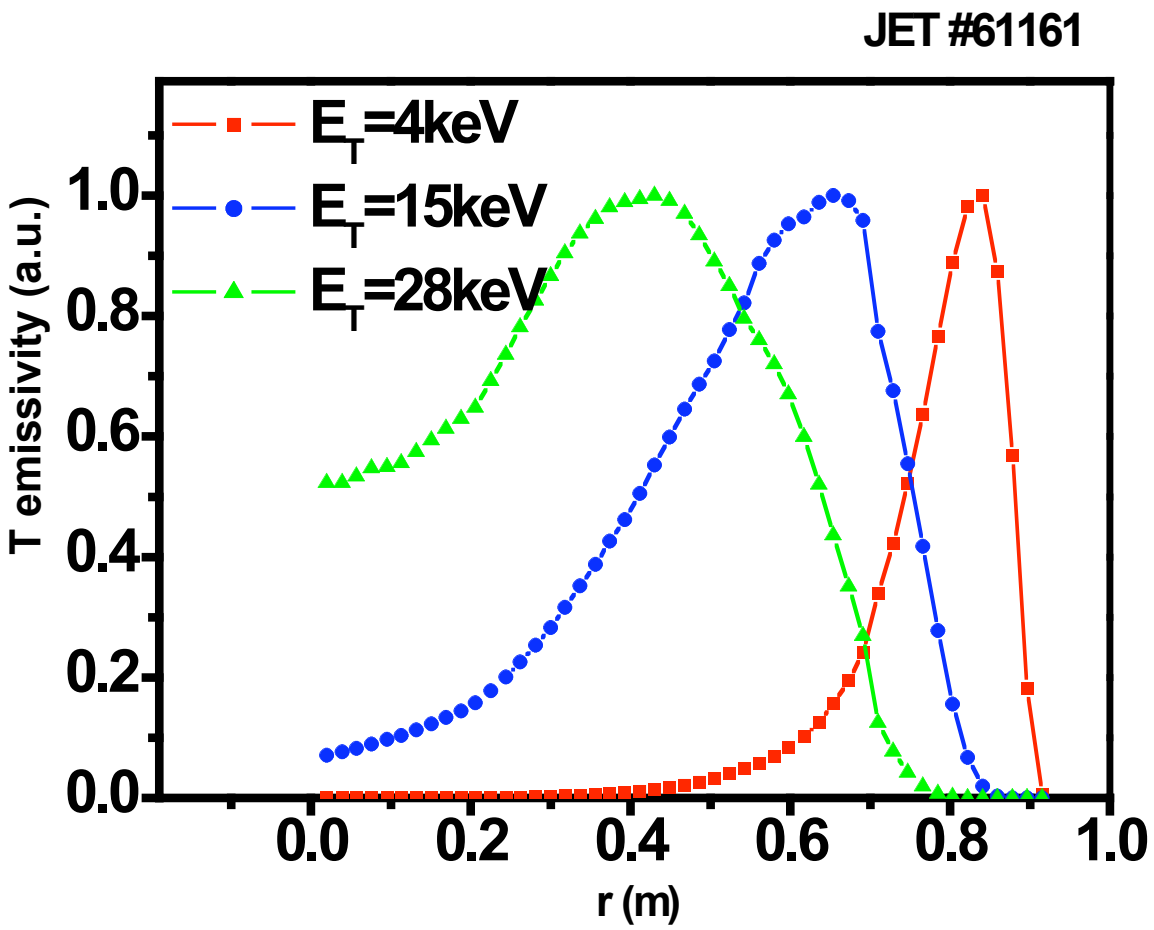

Fig. 17. Calculated source functions for tritium neutral fluxes of different energies [65].

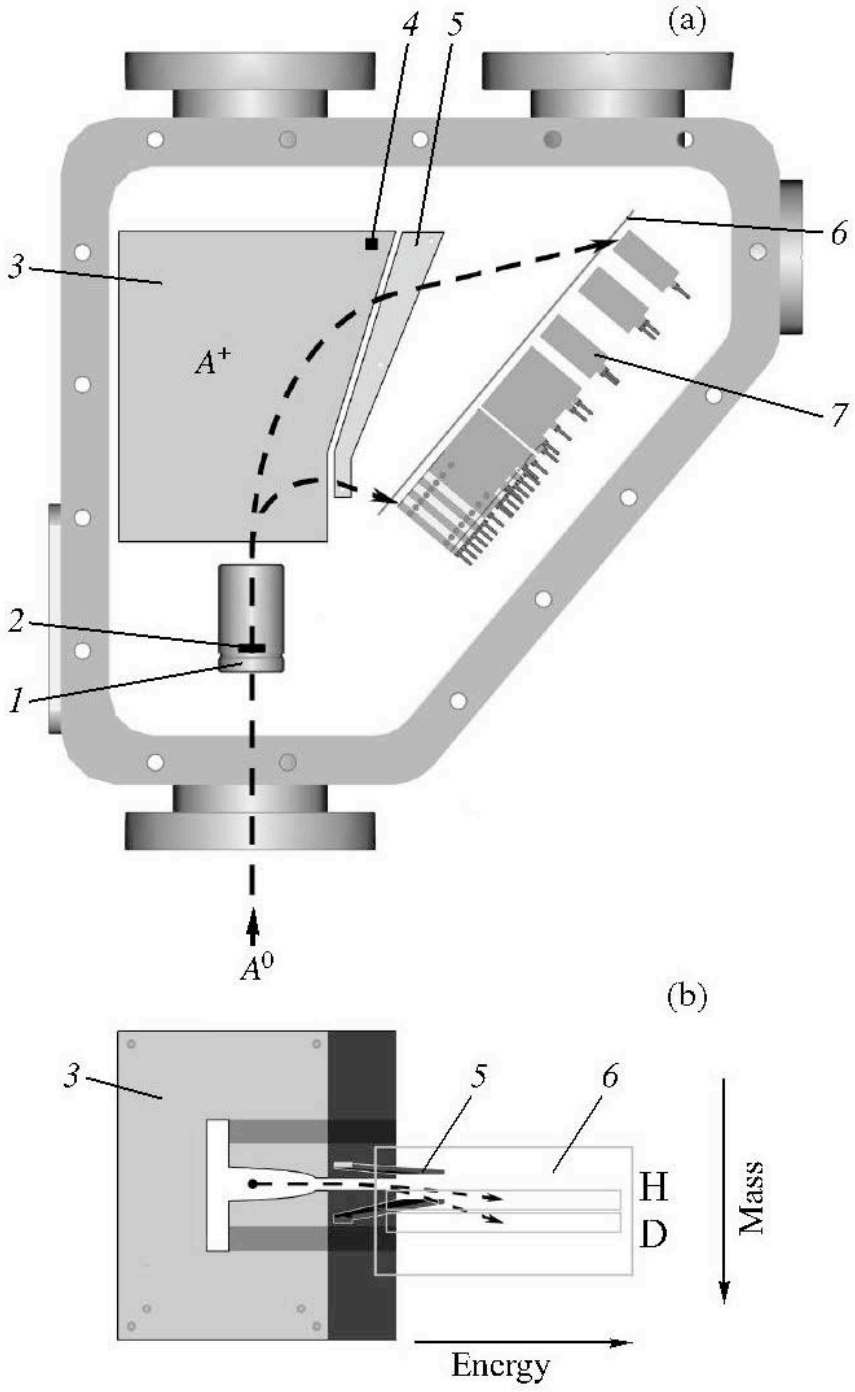

Fig. 18. Diagram of the CNPA analyzer: (1) stripping and acceleration system; (2) stripping foil; (3) analyzing magnet; (4) Hall probe; (5) analyzing electrostatic condenser; (6) shielding mask at the entrance to the detectors; (7) detectors (channeltrons); (A^0) atomic flux emitted by plasma; (A+) secondary ions; (H) hydrogen detector array; and (D) deuterium detector array [66].

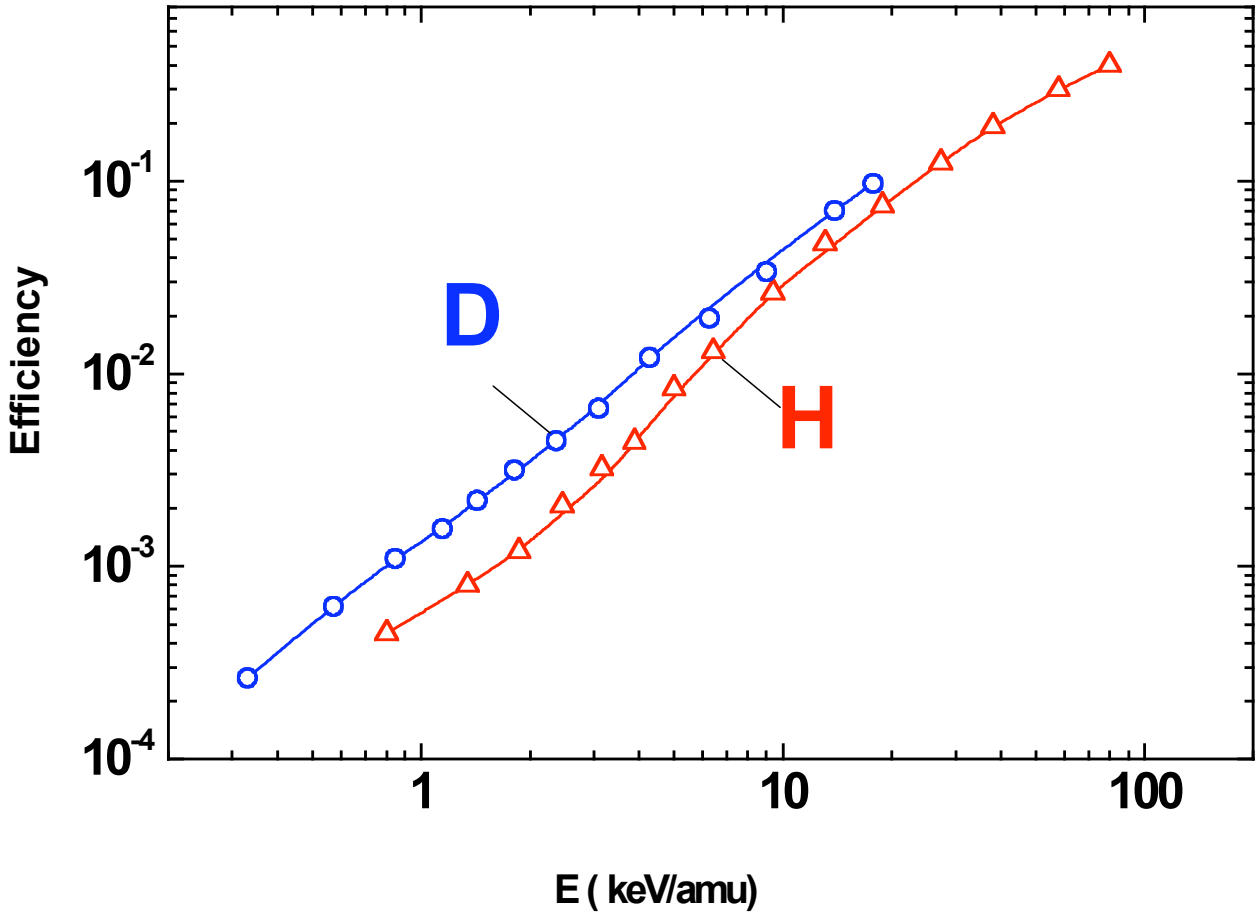

Fig. 19. Shown are the efficiencies for the detection of hydrogen and deuterium atomic fluxes in the CNPA. The electrostatic acceleration of ions scattered by the stripping foil provides focusing of ions before the EIIB dispersion which leads to an increase of the detection efficiency in the energy range E < 1 keV [66].

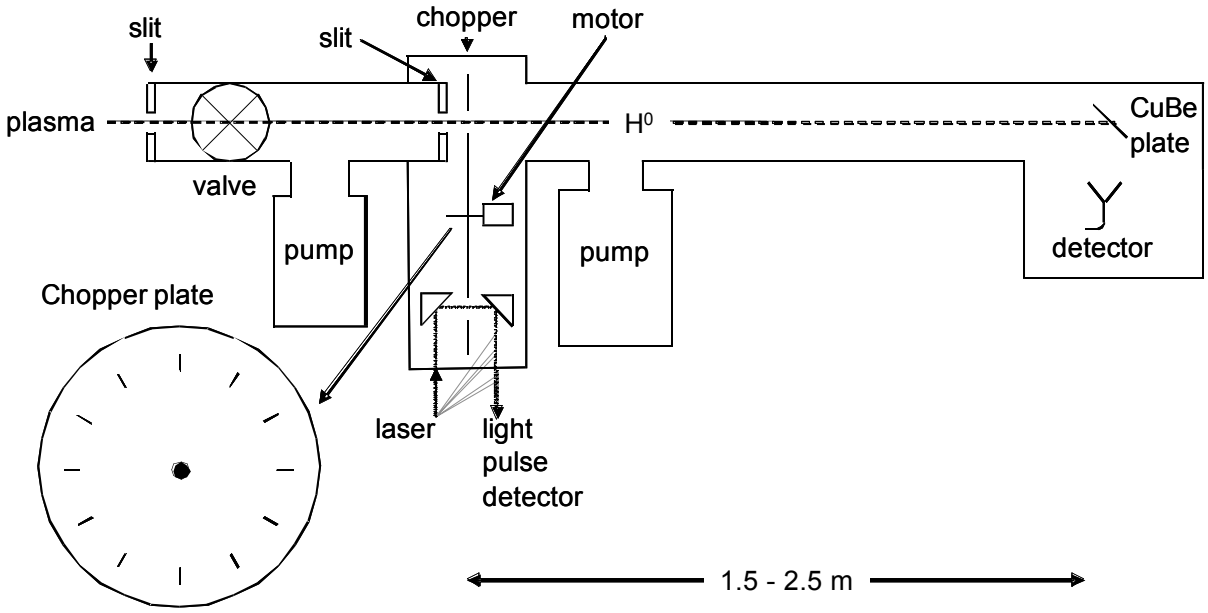

Fig. 20. Schematic drawing of a low-energy time-of-flight analyzer [Donné].

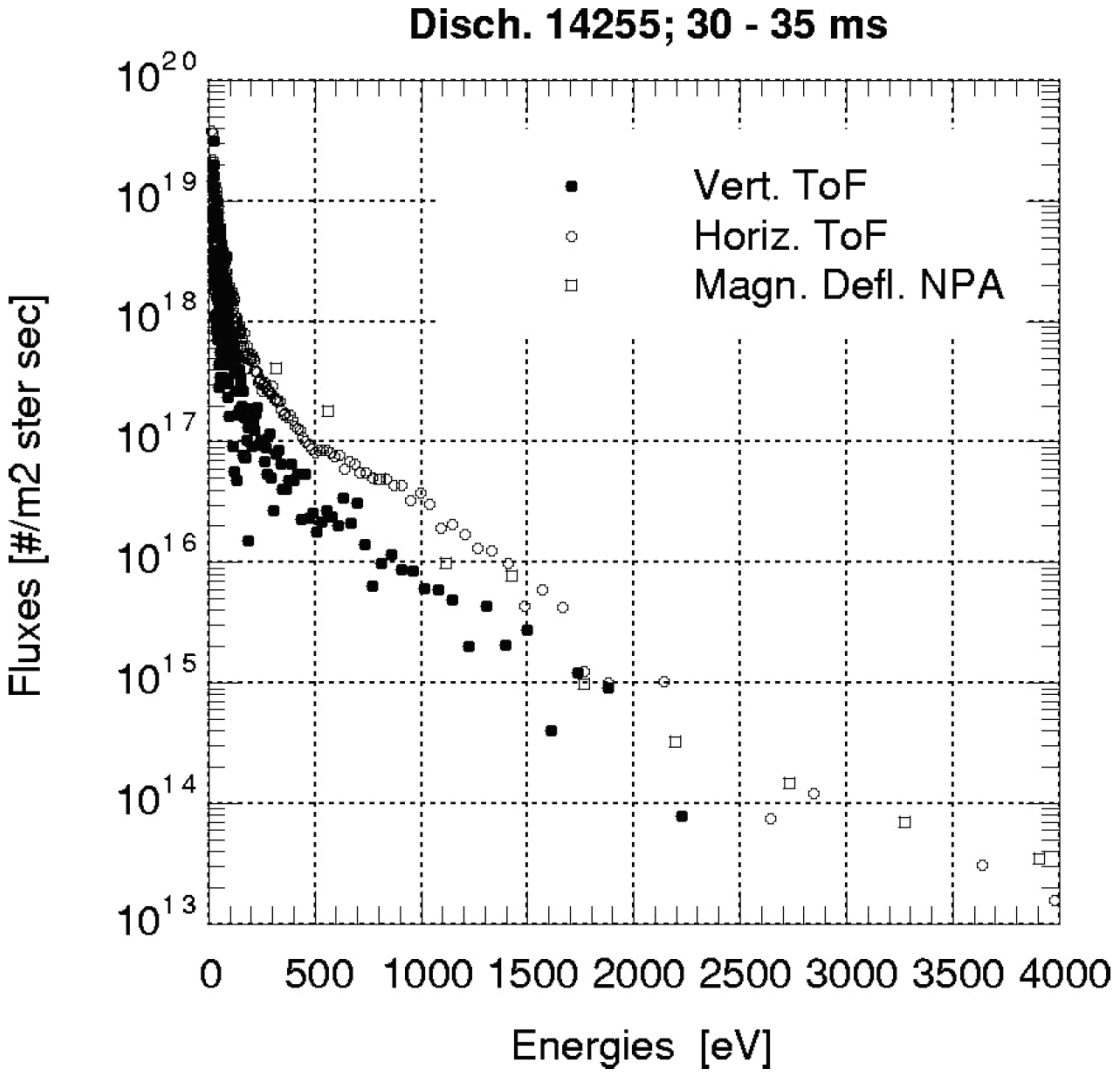

Fig. 21. CX neutral fluxes measured at RFX with a vertical TOF, horizontal TOF and a magnetic NPA for a low-density discharge. The line-of-sight of the vertical system does not pass through the plasma center and therefore the measured fluxes are somewhat lower. Those of the horizontal time-of-flight agree well with the values of the magnetic NPA system in the energy ranger 0.5 – 4 keV [72].

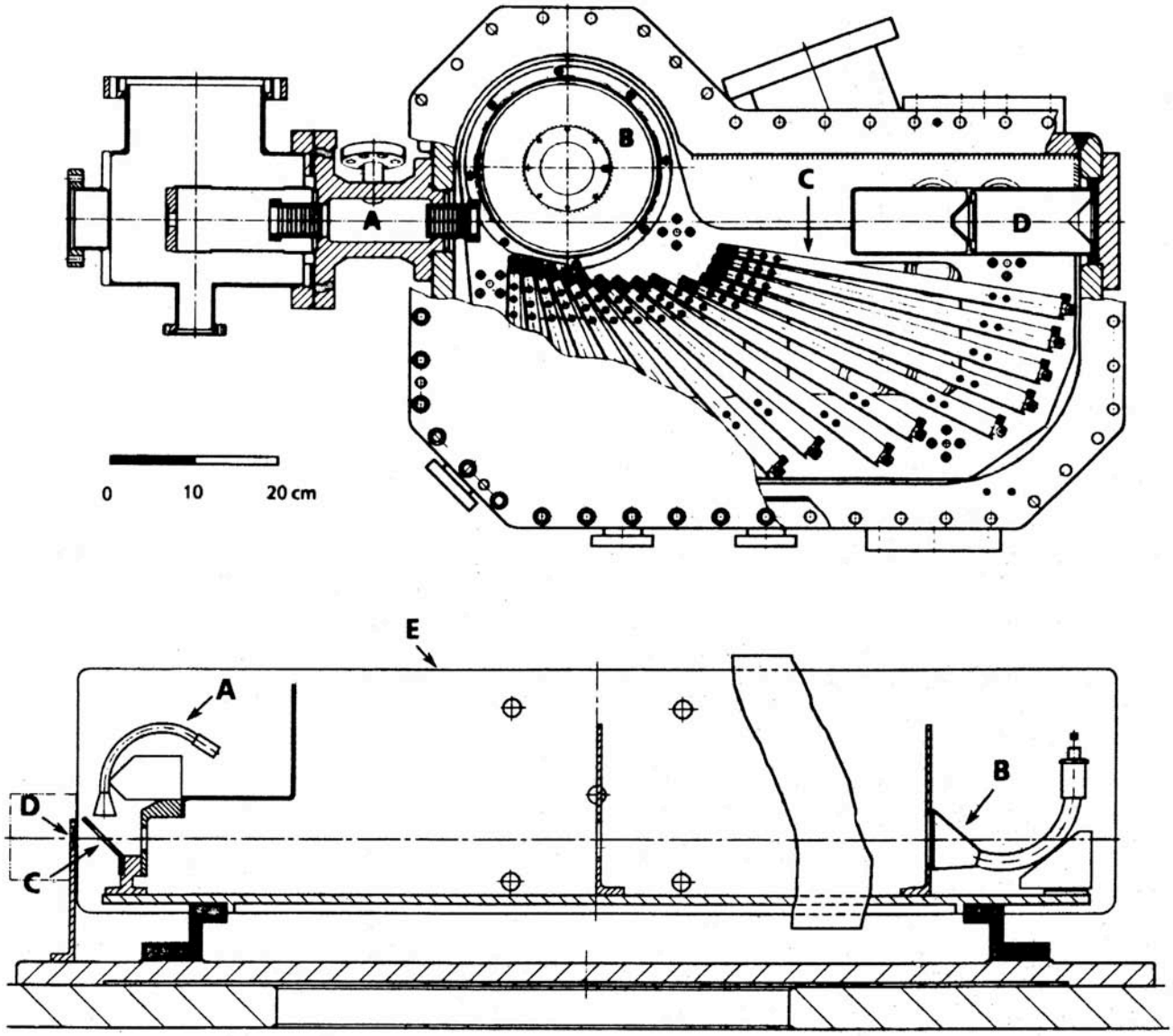

Fig. 22. Layout of the time-of-flight (TOF) type neutral particle analyzer applied at JET. The upper panel shows the mechanical assembly of the analyzer: (A) stripping cell, (B) cylindrical electrostatic plates, (C) TOF detectors, (D) light trap. The lower panel shows the TOF detecting unit: (A) CEM start detector, (B) CEM stop detector, (C) carbon stripping foil, (D) input aperture, (e) μ-metal enclosure [78].

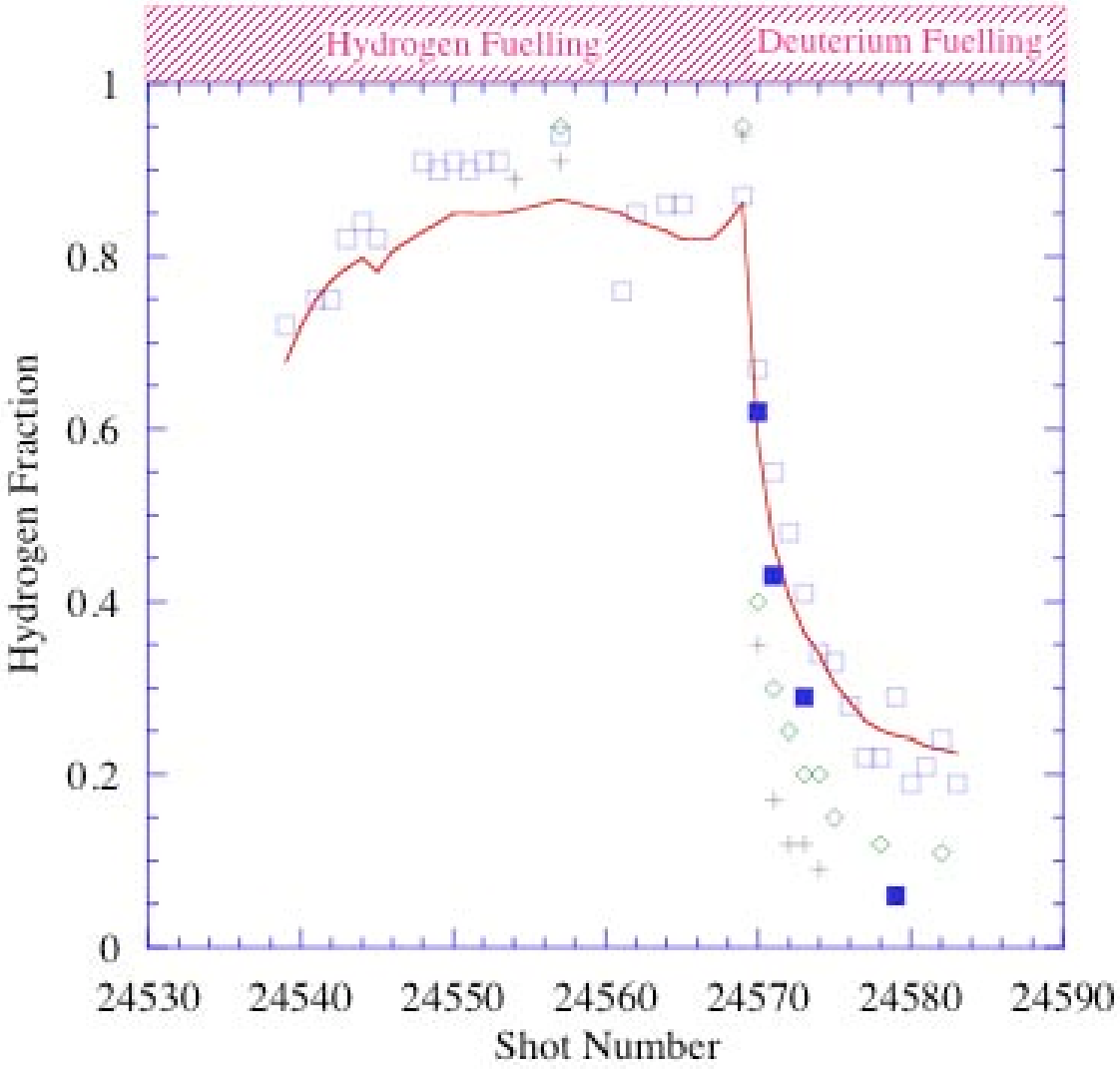

Fig. 23. Measurement of the isotope ratio in JET. The squares have been measured by a quadrupole mass analyzer, the crosses by active Balmer-alpha spectroscopy and the diamonds by the TOF NPA system [83].

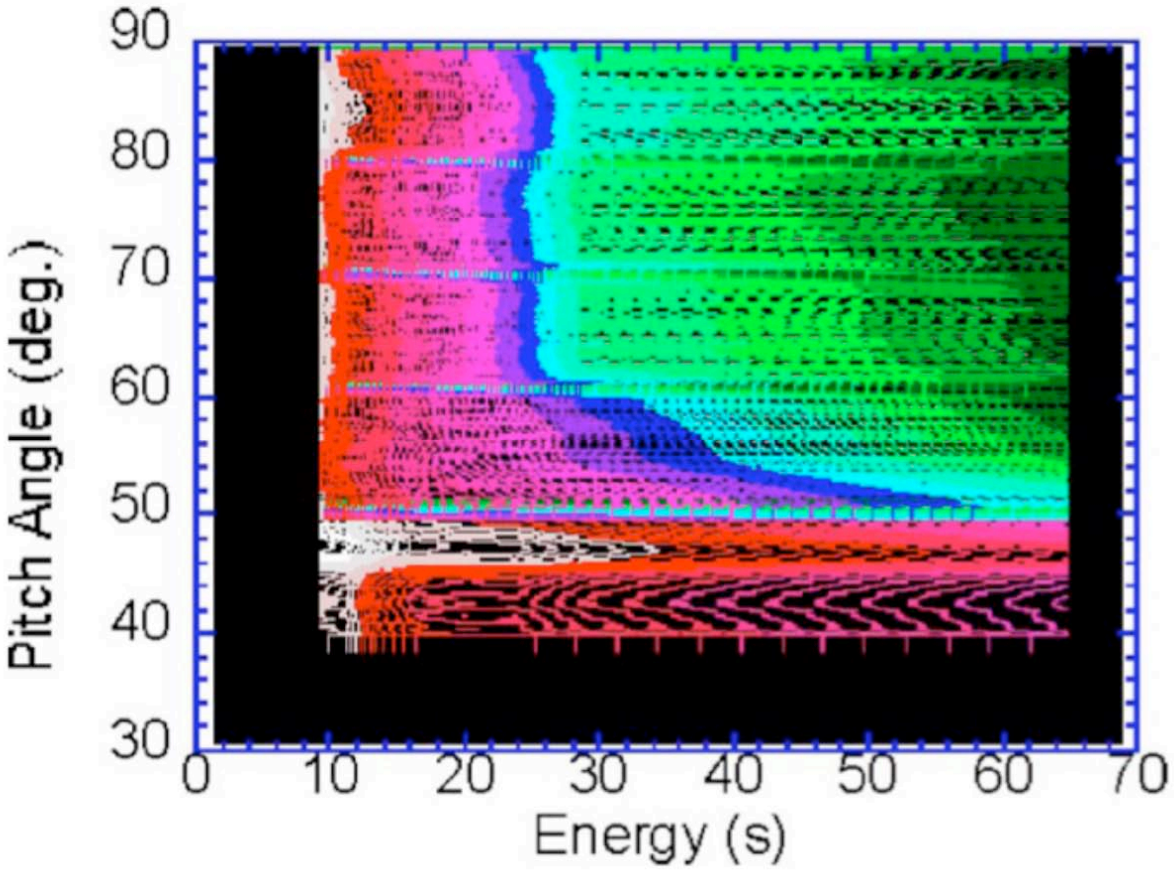

Fig. 24 Contour plot of the pitch angle distribution of neutral particles measured with the TOF analyzer in the stationary phase of a neutral beam heated LHD discharge. The measurement was done in a single discharge with a scan speed of 0.7˚/s. The color indicates the flux of the particles (red = high, green = low). Trapped particles are clearly observed around a 90˚ pitch angle [85].

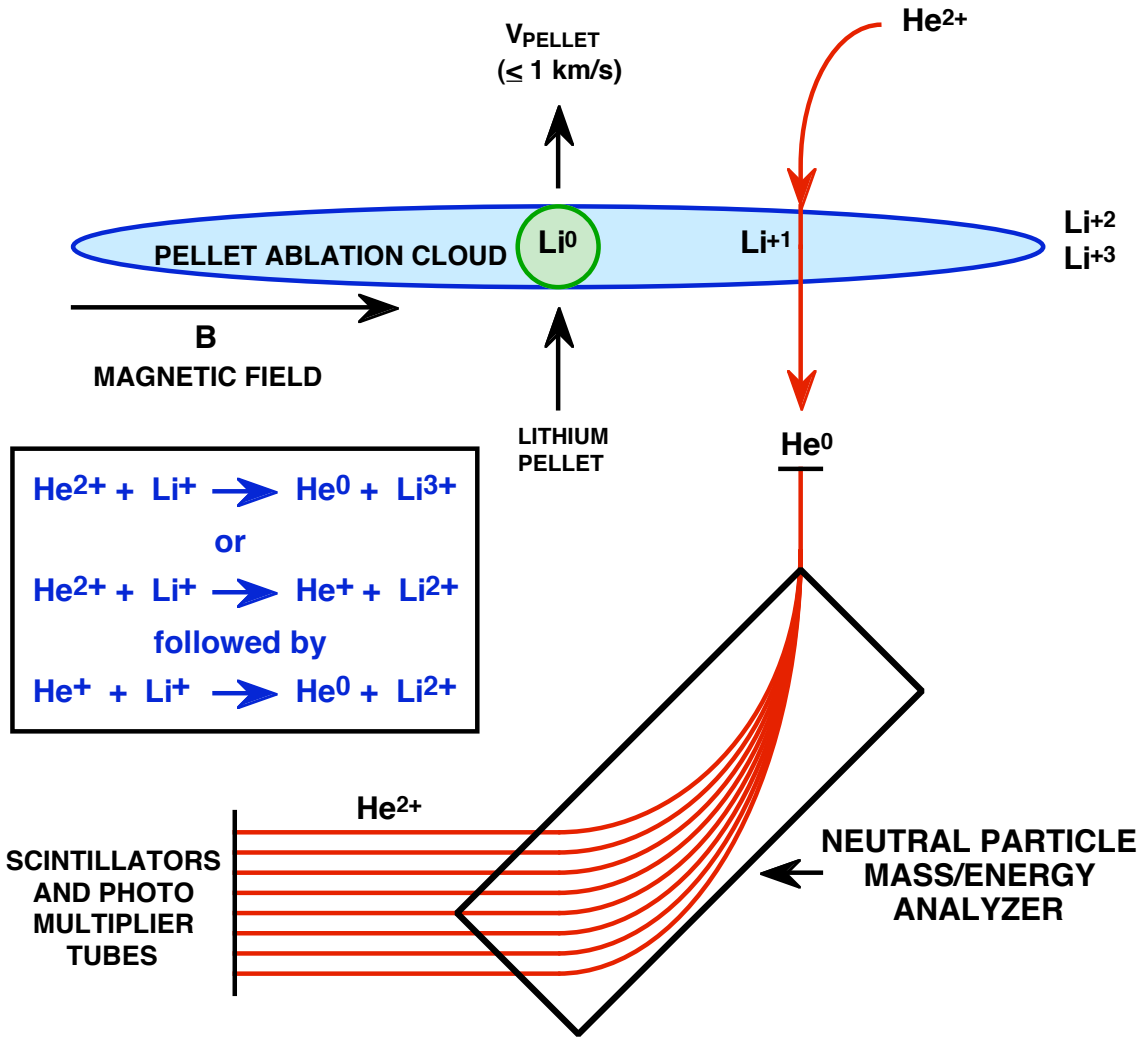

Fig. 25. Illustration of the Pellet Charge Exchange (PCX) concept using lithium as an example of low-Z pellet injection [90].

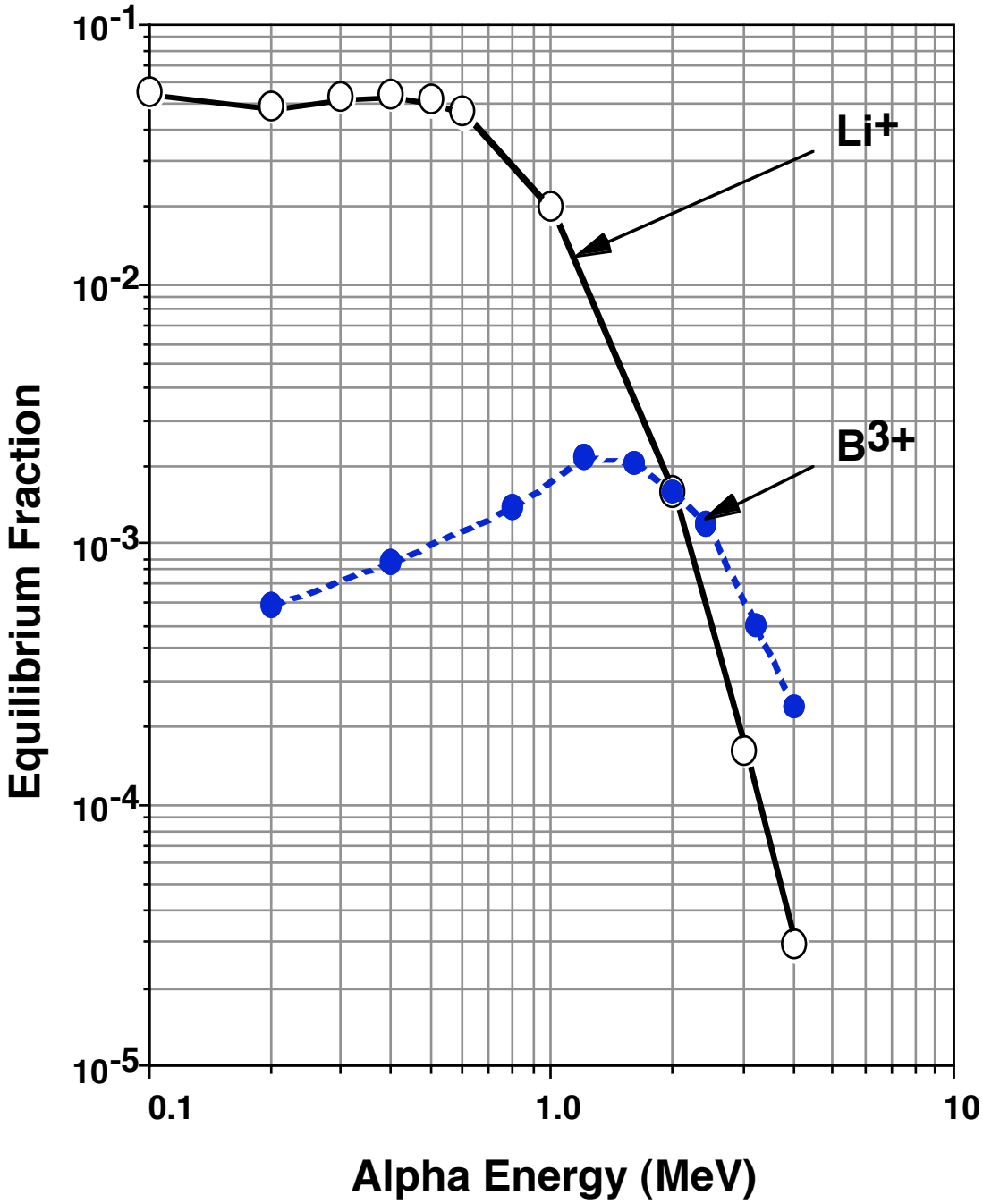

Fig. 26. Calculated neutral equilibrium fractions for alpha particles on helium-like lithium and boron [91].

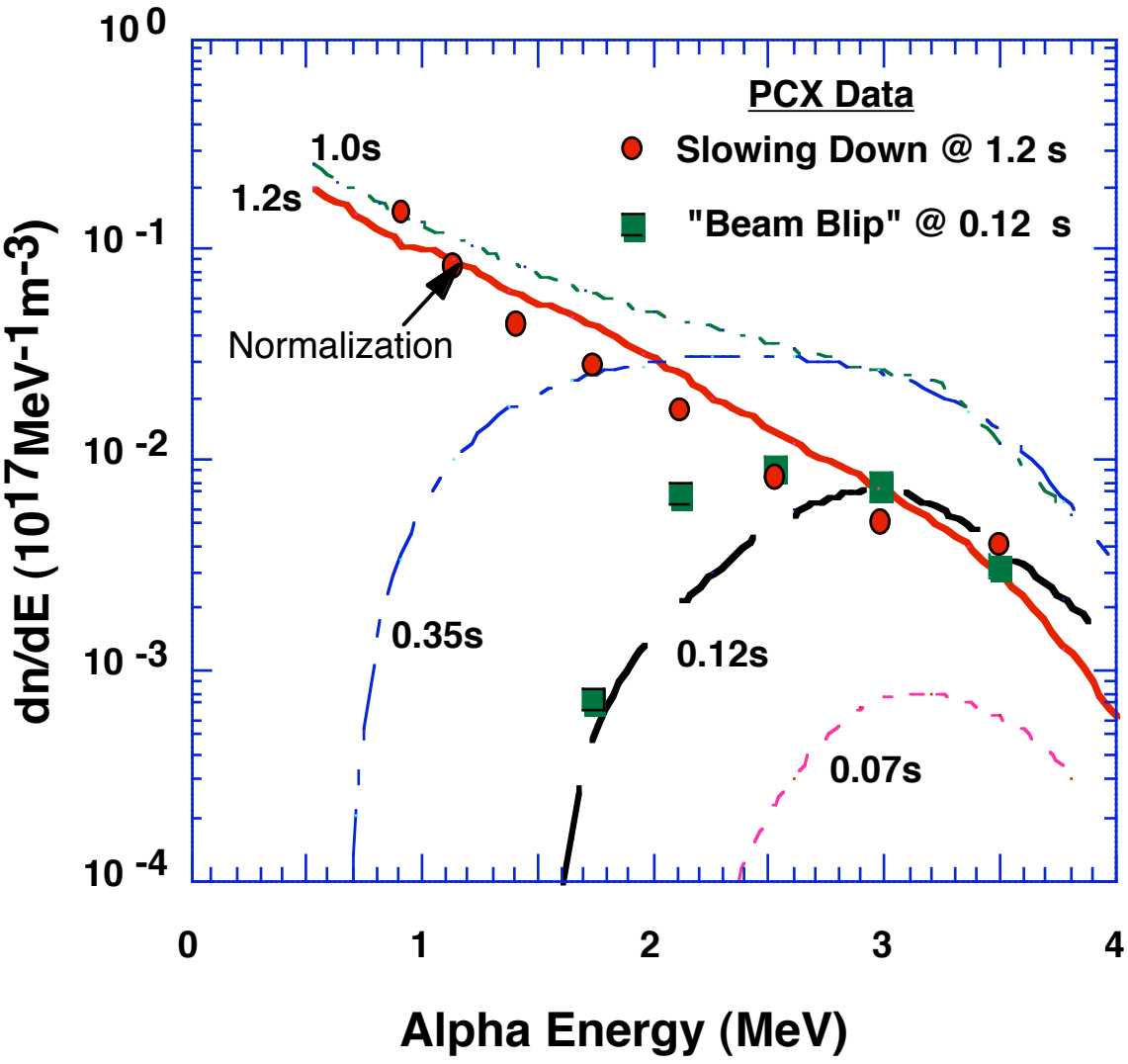

Fig. 27. Shown are alpha spectra measured on TFTR using the Pellet Charge Exchange diagnostic and comparison with the evolution computed using the FPPT code (curves) for two times: (1) near the birth phase shown as full squares corresponding to 0.12 s and (2) during the slowing-down phase shown as full circles corresponding to 1.2 s [91].

The Princeton Plasma Physics Laboratory is operated
by Princeton University under contract
with the U.S. Department of Energy.

Information Services
Princeton Plasma Physics Laboratory
P.O. Box 451
Princeton, NJ 08543

Phone: 609-243-2750
Fax: 609-243-2751
e-mail: pppl_info@pppl.gov
Internet Address: http://www.pppl.gov